

PREPRINT

Author-formatted, not peer-reviewed document posted on 29/04/2025

DOI: <https://doi.org/10.3897/arphapreprints.e156971>

**Diverse metabolites with anti-psoriasis potential from
different fermentations of the fungicolous fungus *Xylaria
longipes* HFG1018**

**Zhen-Zhu Zhao, Yan Wang, Xiao-Yu Wang, Hui Chen, Zhen-Zhen Wang, Jing-Kun Wang, Le-Le Wang,
Ming-Jun Shen, Xin Pang, Wei-Sheng Feng**

1 **Diverse metabolites with anti-psoriasis potential from different**
2 **fermentations of the fungicolous fungus *Xylaria longipes* HFG1018**

3 Zhen-Zhu Zhao¹, Yan Wang¹, Xiao-Yu Wang², Hui Chen¹, Zhen-Zhen Wang², Jing-Kun Wang¹, Le-Le Wang¹,

4 Ming-Jun Shen¹, Xin Pang^{1*}, Wei-Sheng Feng^{1*}

5 ¹ School of Pharmacy, Henan University of Chinese Medicine, Zhengzhou 450046, China

6 ² Academy of Chinese Medical Sciences, Henan University of Chinese Medicine, Zhengzhou 450046, China

7 **Correspondence:**

8 *Xin Pang, Email: pangxin116@163.com

9 *Wei-Sheng Feng, Email: fwsh@hactcm.edu.cn

10

11 **Abstract**

12 The genus *Xylaria* is a promising source of bioactive compounds. This study explored the diversity of
13 secondary metabolites (SMs) in *Xylaria longipes* under three fermentation conditions, isolating 14 new SMs
14 and 27 known ones. The structures were elucidated using NMR, HRESIMS, ROESY, and *J*-based
15 configuration analysis, with absolute configurations determined through calculated ECD and ¹³C NMR data.
16 A comprehensive library of SMs was constructed, facilitating metabolomics-wide association studies that
17 identified culture conditions as a critical factor influencing SM production. This compound library also
18 simplifies the determination of absolute configurations for diplosporins by analyzing *J* values and CD trends.
19 Anti-proliferative assays against induced T/B lymphocytes and HaCaT cells revealed that more than half of
20 the compounds exhibited significant inhibitory activity, with compounds **2**, **15**, and **32** reducing IFN- γ
21 secretion. Compound **32** showed promising anti-psoriatic effects by inhibiting NF- κ B p65 phosphorylation
22 in HaCaT cells. This first systematic chemical study of *X. longipes* under varied conditions provides insights
23 into structure-activity relationships.

24 *Keywords:* *Xylaria longipes*, Xylariaceae, Different fermentation conditions, Chemical investigation;
25 Immunosuppression; HaCaT cells; Psoriasis

26 Introduction

27 Fungi of the genus *Xylaria* are predominantly saprophytic, with a minority exhibiting parasitic behavior.
28 They thrive in forest ecosystems, often near ant colonies or forming symbiotic relationships with plants.
29 These unique ecological niches endow *Xylaria* species with distinct characteristics (Chen et al., 2024).
30 Research has identified terpenoids (Chen et al., 2020, 2024), sterols (Chen et al., 2024), alkaloids (Chen et
31 al., 2024), cyclopeptides (Chen et al., 2024; Li et al., 2011; Wu et al., 2011), and polyketides (Chen et al.,
32 2024; Masahiko et al., 2014; Ibrahim et al., 2014) as the primary chemical constituents produced by *Xylaria*
33 species. Pharmacological studies have demonstrated that extracts or compounds derived from *Xylaria* exhibit
34 a wide range of biological activities, including antioxidant, antibacterial, antitumor, enzyme inhibitory, and
35 immunosuppressive effects, underscoring the genus's significant research value and potential applications
36 (Chen et al., 2024).

37 It is widely recognized that many microbial gene clusters remain silent under standard fermentation
38 conditions. These “silent” or “cryptic” biosynthetic gene clusters may encode novel natural products,
39 representing a vast reservoir of potential drug candidates. The “one strain many compounds” (OSMAC)
40 approach, pioneered by Professor Zeeck and colleagues, involves altering medium composition and other
41 parameters to activate these silent genes, thereby inducing the production of novel secondary metabolites
42 (SMs) (Bode et al., 2002; Pan et al., 2019). This strategy has proven highly effective in unlocking the
43 biosynthesis of cryptic natural products, yielding novel compounds with significant potential (Pfütze et al.,
44 2024; Zhang et al., 2015).

45 *Xylaria longipes* HFG1018, isolated from the medicinal fungus *Fomitopsis betulina* (Bull.)
46 (Fomitopsidaceae), is a typical ectomycorrhizal fungus within the Xylariaceae family. Fungicolous fungi
47 (FF), having co-evolved with their hosts through long-term natural selection, provide valuable insights into
48 host-fungus interactions through the study of their SMs (Sun et al., 2019). Previous research on *X. longipes*
49 HFG1018 led to the isolation of a series of nor-pimarane diterpenes and two novel bicyclo (2.2.2) octane
50 diterpene skeletons with immunosuppressive properties from its liquid fermentation (Chen et al., 2020). To
51 further explore its chemical diversity, three distinct fermentation systems were employed in this study,
52 resulting in the isolation of 14 new compounds, including three pimarane-type diterpenes (1–3), one
53 pentapeptide (4), nine 6-ethyl 4*H*-chromen-4-one derivatives (diplosporins) (5–13), and one isochromone

54 (14), alongside 27 known compounds (Figs. 1 and 2). Notably, all new SMs were obtained from rice
55 fermentation. Among these, compound 1 represents the first example of a 6/6/6/6-fused tetracyclic pimarane;
56 compound 4 is a rare pentapeptide; and compound 9 is a novel nordiplosporin.

57 Psoriasis is an almost incurable skin disease with excessive immune response and over-proliferation of
58 keratinocytes. Antiproliferative assays against induced-T/B lymphocytes (immune cells) and a keratinocyte
59 cell line (HaCaT) revealed that several compounds are promising for anti-psoriasis activity. This study details
60 the isolation, structural elucidation, and bioactivity evaluation of these metabolites, contributing to the
61 growing knowledge on *Xylaria* species and their potential applications.

62 **Methods and materials**

63 **General experimental procedures**

64 Optical UV spectra were recorded on a Shimadzu UV-2401PC UV-visible recording spectrophotometer
65 (Shimadzu, Kyoto, Japan). IR spectra (in MeOH) were measured on a Bruker Tensor 27 spectrometer (Bruker,
66 Karlsruhe, Germany). Rotations were calculated using the APIV (Rudolph Research Analytical). All the
67 NMR spectra were obtained on a Bruker Avance III 500 MHz spectrometer (Bruker Corporation, Karlsruhe,
68 Germany). High-resolution electrospray ionization mass spectra (HRESIMS) were recorded using an AB
69 Sciex Triple-TOF 6600 (AB SCIEX, Framingham, MA, USA). Macroporous adsorption resin (Cangzhou
70 Bon Adsorber Technology Co., Ltd, Cangzhou, China), Sephadex LH-20 (Amersham Biosciences, Uppsala,
71 Sweden), and silica gel (Qingdao Haiyang Chemical Co., Ltd, China) were used for column chromatography
72 (CC). Medium-pressure liquid chromatography (MPLC) was performed on the FL-H050G MPLC system
73 (Agela Technologies, Tianjin, China) with an Agela ODS flash column (C-18, 120 g, 40–60 mm, Tianjin,
74 China) or MCI gel (CHP20/P120, Mitsubishi Chemical Corporation, Yokohama, Japan). Preparative high-
75 performance liquid chromatography (prep. HPLC) was performed on a SEP LC-52 equipped with a YMC-
76 pack ODS-A column (dimensions 250 × i.d. 10 mm, particle size 5 μm, 4 mL/min; dimensions 250 × i.d.
77 20 mm, particle size 5 μm, 7 mL/min; YMC, Tokyo, Japan), and a MWD UV detector (Separation
78 Technology Co Ltd., Beijing, China). All solvents used were of analytical or Chromatographic grades
79 (TJshield Fine Chemicals Co., Ltd, Tianjin, China). All elution systems were described in terms of volume
80 ratio. Concanavalin A (ConA), lipopolysaccharide (LPS, Escherichia coli 055: B5), CCK-8, and RPMI
81 1640/DMEM media were purchased from Solarbio Life Sciences (Beijing, China). Fetal bovine serum (FBS)

82 was purchased from HyClone Laboratories (Utah, USA). All elution systems were described in terms of
83 volume ratio.

84 **Fungal material and taxonomy**

85 ***Sample collection and morphological characterization***

86 The fungus *Xylaria longipes* HFG1018 (Xylariaceae) was isolated from the wood-rotting fungus *Fomitopsis*
87 *betulina* (Bull.) (Fomitopsidaceae). *F. betulina* was harvested from Changbai Mountain National Nature
88 Reserve, Jilin Province, China, in 2012 and identified by the ITS gene (GenBank accession No. PQ844712).
89 The fungus *Xylaria longipes* was confirmed by combing analysis of the ITS gene (GenBank accession No.
90 PV523290), *TUB2* gene (GenBank accession No. MN583256), and *rpb2* gene (GenBank accession No.
91 PV558833). The sample was preserved in the Department of Traditional Chinese Medicine and Natural
92 Medicinal Chemistry, Henan University of Traditional Chinese Medicine (No. HFG1018).

93 Pure cultures were maintained at 25 °C for 1-4 weeks on oatmeal agar (OA) medium. The mycelium,
94 stained with methylene blue, is examined for microscopic features under a biological microscope. Micro
95 characteristics were observed under an ML11-II biomicroscope (Guangzhou Mingmei Optoelectronic
96 Technology Co., Ltd, China) and photographed by an iPhone 13 Pro camera.

97 ***Sequence alignments and phylogenetic analyses***

98 All the obtained sequences were deposited in GenBank (Table S1, Supplementary Information). The
99 obtained sequences were analyzed using the BLAST tool in NCBI GenBank to search for highly similar
100 sequences. Single sequences (ITS, *TUB2*, and *rpb2*) were aligned with the Clustal W algorithm in the MEGA
101 v.12 program and manually adjusted for maximum sequence similarity. Multiple sequences were
102 concatenated using PhyloSuite software (Zhang et al. 2020). Phylogenetic trees were constructed using
103 concatenated sequences (ITS, *TUB2*, and *rpb2*) in MEGA v.12 with the neighbor-joining (NJ) and maximum-
104 likelihood (ML) methods. The multi-locus phylogenetic tree included the fungal isolate studied here and
105 other closely related species of the *Xylaria* genus, with *Engleromyces sinensis* and *Collodiscula bambusae*
106 serving as an outgroup. Clade stability was evaluated with 1 000 bootstrap replicates.

107 **Fermentation, extraction, and isolation**

108 ***Rice fermentation***

109 Rice fermentation was conducted following established protocols. The glucose peptone yeast (GPY) medium

110 used for fermenting *X. longipes* contained glucose (5%), peptone from porcine meat (0.15%), yeast powder
 111 (0.5%), KH₂PO₄ (0.05%), and MgSO₄ (0.05%). Two bottles of GPY liquid fermentation medium (350
 112 mL/bottle) inoculated with *X. longipes* were incubated in a shaker at 24°C and 150 rpm for 7 days in the
 113 dark. Separately, rice and distilled water (H₂O) were mixed at a mass ratio of 1:1.3 (total rice weight: 20 kg)
 114 and distributed into 500 mL flasks, which were then autoclaved. The cultured liquid mycelium was
 115 subsequently transferred into the sterilized flasks and incubated in the dark for 40 days.

116 After fermentation, the rice substrate was transferred to an extraction tank and subjected to ultrasound-
 117 assisted extraction with 95% ethanol for 3 hours per cycle. This process was repeated three times. The ethanol
 118 solution containing metabolites was concentrated under reduced pressure until only water remained. The
 119 aqueous concentrate was then extracted four times with an equal volume of ethyl acetate (EtOAc). The
 120 EtOAc layer was concentrated under reduced pressure to yield 233.9 g of crude extract. This crude extract
 121 was further fractionated using macroporous adsorption resin column chromatography (CC) with a gradient
 122 of EtOH–H₂O (20:80, 40:60, 60:40, 80:20, 100:0), resulting in nine fractions (A–I).

123 Fractions B–D (68.3, 14.8, and 4.2 g, respectively) and fraction F (27.9 g) were further separated using
 124 medium-pressure liquid chromatography (MPLC). Fractions B–D were processed on an MCI gel column,
 125 while fraction F was separated on a C18-ODS column, both employing a gradient elution of methanol
 126 (MeOH) in H₂O (20:80, 40:60, 60:40, 80:20, 100:0). This yielded four to six subfractions for each fraction
 127 (B1–B4, C1–C5, D1–D7, and F1–F6, respectively).

128 Subfraction B2 was subjected to Sephadex LH-20 column chromatography using MeOH as the eluent,
 129 resulting in six parts (B2a–B2f). Compounds **5** (286.8 mg, *t_R* = 20.7 min) and **6** (57.0 mg, *t_R* = 20.0 min)
 130 were purified from fraction B2d using preparative HPLC with a gradient of acetonitrile (MeCN)/H₂O
 131 (15:85→100:0, 50 min, 4 mL/min).

132 Subfraction C1 was fractionated into three parts (C1a–C1c) via Sephadex LH-20 (MeOH). Fraction C1a
 133 was further separated using Sephadex LH-20 (acetone), yielding four subfractions (C1a1–C1a4). Fraction
 134 C1a1 was separated by prep. HPLC (MeCN/H₂O 35:65→80:20→100:0, 0→50→60 min, 4 mL/min) to give
 135 compounds **23** (16.5 mg, *t_R* = 14.7 min) and **25** (347.9 mg, *t_R* = 13.0 min). Fraction C1a2 was eluted on a
 136 silica gel CC with an isocratic elution of petroleum ether–acetone (1:1) to afford four components (C1a2a–
 137 C1a2d). Compounds **7** (61.1 mg, *t_R* = 17.3 min) and **11** (5.1 mg, *t_R* = 28.2 min) were purified from fraction

138 C1a2a using prep. HPLC (MeCN/H₂O 20:80→70:30, 60 min, 4 mL/min). Compounds **22** (2.9 mg, $t_R = 30.8$
 139 min) and **14** (1.5 mg, $t_R = 31.9$ min) were isolated from fraction C1a2c via prep. HPLC with an isocratic
 140 elution of MeCN/H₂O (30:70, 4 mL/min). Fraction C1a2d was separated via prep. HPLC (MeOH/H₂O
 141 50:50→100:0, 30 min, 8 mL/min), yielding three components (C1a2d1–C1a2d3). Compounds **26** (7.4 mg,
 142 $t_R = 16.5$ min), **9** (6.7 mg, $t_R = 36.9$ min), and **12** (17.4 mg, $t_R = 41.1$ min) were obtained from fraction C1a2d1.

143 Fraction C2 was separated on silica gel CC with an isocratic elution of petroleum ether–acetone (1:1),
 144 yielding two components (C2a and C2b). Compounds **10** (58.6 mg, $t_R = 28.8$ min), **7** (7.3 mg, $t_R = 29.7$ min),
 145 and **24** (43.6 mg, $t_R = 39.2$ min) were purified from fraction C2a using prep. HPLC (MeCN/H₂O
 146 25:75→100:0, 50 min, 4 mL/min).

147 Fraction D5 was separated using MPLC equipped with a C18-ODS column, employing a gradient elution
 148 of MeOH in H₂O (20:80, 40:60, 60:40, 80:20, 100:0), resulting in six subfractions (D5a–D5f). Fraction D5b
 149 was further purified using Sephadex LH-20 (MeOH), yielding three components (D5b1–D5b3). Compound
 150 **19** (4.7 mg, $t_R = 23.8$ min) was obtained from fraction D5b3 via prep. HPLC (MeCN/H₂O 30:70→100:0, 50
 151 min, 4 mL/min).

152 Fractions F1 to F4 were subjected to Sephadex LH-20 (MeOH) chromatography, yielding three or four
 153 components each (F1a–F1c, F2a–F2c, F3a–F3c, and F4a–F4d). Compound **20** (30.2 mg, $t_R = 28.5$ min) was
 154 isolated from fraction F1b using prep. HPLC (MeCN/H₂O 15:85→40:60, 70 min, 3 mL/min). Compounds
 155 **21** (34.3 mg, $t_R = 35.0$ min) and **28** (2.4 mg, $t_R = 37.6$ min) were obtained from fraction F2c via prep. HPLC
 156 with an isocratic elution of MeCN/H₂O (30:70, 3 mL/min). Compound **27** (3.4 mg, $t_R = 24.7$ min) was
 157 obtained from fraction F3c using prep. HPLC (isocratic elution of MeOH/H₂O 71:29, 7 mL/min). Compound
 158 **3** (4.9 mg, $t_R = 35.1$ min) was isolated from fraction F4b via prep. HPLC (MeCN/H₂O 20:80→60:40, 55 min,
 159 4 mL/min).

160 Fraction F5 was separated using MPLC equipped with an MCI gel column by a gradient eluent of MeOH
 161 in H₂O (20:80, 40:60, 60:40, 80:20, 100:0), yielding seven subfractions (F5a–F5g). Fractions F5d, F5f, and
 162 F5g were dealt with Sephadex LH-20 (MeOH), resulting in three or five components each (F5d1–F5d3,
 163 F5f1–F5f5, and F5g1–F5g5). Compounds **16** (141.8 mg, $t_R = 10.6$ min), **17** (72.2 mg, $t_R = 43.9$ min), and **2**
 164 (16.6 mg, $t_R = 44.6$ min) from fraction F5d2 via prep. HPLC (isocratic elution of MeCN/H₂O 42:58, 4
 165 mL/min). Compound **4** (7.44 mg, $t_R = 24.5$ min) was obtained from fraction F5f1 using prep. HPLC

166 (MeCN/H₂O 38:62 → 70:30, 40 min, 4 mL/min). Compound **15** (8.7 mg, $t_R = 16.5$ min) was purified from
 167 fraction F5f4 using prep. HPLC (MeCN/H₂O 62:38, 4 mL/min). Compound **18** (41.5 mg, $t_R = 9.8$ min) was
 168 isolated from fraction F5g2 using prep. HPLC (MeCN/H₂O 60:40→100:0, 20 min, 4 mL/min). Compound
 169 **29** (2.3 mg, $t_R = 12.5$ min) from fraction F5g3 using prep. HPLC (MeCN/H₂O 60:40→100:0, 20 min, 4
 170 mL/min). Finally, compound **1** (1.3 mg, $t_R = 17.5$ min) was purified from fraction F5g5 using prep. HPLC
 171 (60:40→100:0, 20 min, 4 mL/min).

172 *Liquid fermentation of potato dextrose broth (PDB)*

173 The culture medium for fermenting *X. longipes* was prepared using potato (200 g), peptone from porcine
 174 meat (1.0 g), dextrose (20.0 g), KH₂PO₄ (3.0 g), and MgSO₄ (1.5 g) dissolved in deionized H₂O (1.0 L). A
 175 total of 20 L of the culture medium was inoculated with the *X. longipes* strain and incubated at 24 °C with
 176 shaking at 150 rpm on rotary shakers for 28 days in a dark environment. After 7 days of fermentation, 3-
 177 methyl-2-butenol was added to the broth at a 400 mg/L concentration.

178 Following fermentation, the 20.0 L broth was separated into supernatant and mycelia by centrifugation.
 179 The supernatant was concentrated under reduced pressure, and the resulting residue was partitioned between
 180 ethyl acetate (EtOAc) and H₂O. Simultaneously, the mycelia were extracted three times with ethanol (EtOH).
 181 The EtOH extract was evaporated and similarly partitioned between EtOAc and H₂O four times. The
 182 combined EtOAc layers yielded a total weight of 24 g.

183 The EtOAc extract underwent MPLC using a C18-ODS column, eluted by a gradient eluent of MeOH in
 184 H₂O (20:80, 40:60, 60:40, 80:20, 100:0), yielding five fractions (A–E). Fractions B (5.6 g) and D (9.7 g)
 185 were separated over silica gel CC eluted with petroleum ether–acetone (2:1, 1:1, 0:1), giving 12 (B1–B12)
 186 and eight fractions (D1–D8). Compound **30** (178.6 mg, $t_R = 27.9$ min) was purified from fraction B2 via
 187 prep. HPLC (MeCN/H₂O 34:66→69:31→100:0, 0→35→45 min, 4 mL/min).

188 Subfraction D4 was further purified by preparative prep. HPLC using a gradient eluent (MeCN/H₂O
 189 80:20→100:0, 15 min, 4 mL/min) to afford compounds **31** (4.1 mg, $t_R = 27.9$ min) and **33** (1.3 mg, $t_R = 40.5$
 190 min). Fraction D2 was subjected to prep. HPLC (MeCN/H₂O 51:49→95:5, 35 min, 4 mL/min) gives 12
 191 components (D2a–D2l). Compounds **34** (1.2 mg, $t_R = 38.4$ min) from fraction D2e (MeCN/H₂O
 192 60:40→100:0, 45 min, 4 mL/min) and **32** (4.0 mg, $t_R = 43.5$ min) from fraction D2h (MeCN/H₂O
 193 80:20→100:0, 45 min, 4 mL/min) via prep. HPLC.

194 **Liquid fermentation of glucose peptone yeast (GPY)**

195 45.0 L of the GPY culture medium was inoculated with *X. longipes* strain and was then incubated at 24 °C
 196 and 150 rpm on rotary shakers for 28 days in a dark environment. After fermentation for 7 days, 3-methyl-
 197 2-butenol was added (400 mg/ L).

198 After a procedure similar to PDB fermentation, 45.0 L GPY fermentation, and mycelium gave an EtOAc
 199 layer (41.5 g). The EtOAc extract underwent macroporous adsorption resin CC eluted with an EtOH/H₂O
 200 gradient (20:80, 40:60, 60:40, 80:20, 100:0), yielding four fractions (A–D). Fraction C (3.4 g) was separated
 201 on MPLC (C18-ODS column) and eluted with a MeOH/H₂O gradient (20:80, 40:60, 60:40, 80:20, 100:0),
 202 yielding eight fractions (C1–C8). Fractions C3 (MeOH/H₂O, 20:80→100:0, 30 min, 7 mL/min) and C6
 203 (MeOH/H₂O 50:50→100:0, 45.0 min, 7 mL/min) were further separated over prep. HPLC to provide eight
 204 (C3a–C3h) or three fractions (C6a–C6c), respectively. Compounds **37** (2.6 mg, *t_R* = 8.7 min) from fraction
 205 C3d (MeCN/H₂O 22:78, 4 mL/min), **39** (4.6 mg, *t_R* = 14.5 min) from fraction C3h (MeCN/H₂O 20:80→50:50,
 206 30 min, 4 mL/min), **38** (2.4 mg, *t_R* = 10.4 min) from fraction C6b (MeCN/H₂O 35:65→65:35→100:0,
 207 0→35→50 min, 3 mL/min), and **41** (5.5 mg, *t_R* = 28.9 min) from fraction C6c (MeCN/H₂O
 208 35:65→65:35→100:0, 0→35→50 min, 4 mL/min) were purified by prep. HPLC. Fraction C5 was separated
 209 on MPLC (MCI gel column) eluted with a MeOH/H₂O gradient (20:80, 40:60, 60:40, 80:20, 100:0), yielding
 210 six fractions (C5a–C5f). Compounds **36** (9.7 mg, *t_R* = 8.7 min) from fraction C5c
 211 (MeCN/H₂O 15:85→70:30→100:0, 0→30→60 min, 4 mL/min), **40** (4.4 mg, *t_R* = 35.3 min) from fraction
 212 C5e (MeCN/H₂O 35:65→60:40→100:0, 0→60→80 min, 4 mL/min), and **28** (2.4 mg, *t_R* = 38.2 min)/**35** (2.4
 213 mg, *t_R* = 51.2 min) from fraction C5g (MeCN/H₂O 28:72→28:72→100:0, 0→60→70 min, 4 mL/min) were
 214 obtained via prep. HPLC. Fraction D (2.6 g) was subjected to silica gel CC, using a petroleum ether–acetone
 215 elution system (2:1, 1:1, 0:1), giving six fractions (D1–D6), and then subfraction D1 was dealt with prep.
 216 HPLC (MeCN/H₂O 40:60→75:25→100:0, 0→30→45 min, 4 mL/min) to give compound **25** (4.5 mg, *t_R* =
 217 23.5 min)

218 **Calculations of ¹³C NMR and ECD**

219 Conformational analysis of the candidate structures (compounds **1**, **5**, **6**, **13**, and **14**) was performed using
 220 the MMFF94s force field. The conformers with a distribution greater than 1% were further optimized at the
 221 B3LYP/6-31G(d,p) level of theory in the Gaussian 16 software package. The optimized conformers within

222 3 kcal·mol⁻¹ of the global minimum were selected for additional ¹³C NMR (**1**, **13**) and ECD (**1**, **5**, **6**, **13**, and
223 **14**) calculations (Supplementary Information).

224 ¹³C NMR calculation. Gauge-independent atomic orbital (GIAO) calculations of the shielding values of
225 candidates were accomplished by the time-dependent density functional theory (TDDFT) at the
226 mPW1PW91/6-31G(d,p) level in CHCl₃ with the IEFPCM model in the Gaussian 16 software package
227 (Frisch et al. 2016). The calculated NMR data of these conformers were averaged according to the Boltzmann
228 distribution theory and their relative Gibbs free energies. The correlation coefficient (R^2) and mean absolute
229 error (MAE) were calculated to evaluate the deviations between the experimental and calculated results. The
230 calculation results were processed by an in-house Excel-based program.

231 ECD calculation. The theoretical calculations of ECD were performed using TDDFT at B3LYP/6-
232 31G(d,p) level in MeOH with the CPCM model in the Gaussian'16 software package. The calculated ECD
233 curve was generated using SpecDis 1.70.1. The ECD curve of the enantiomers was generated by the function
234 "enantiomeric ECD" in SpecDis (Bruhn et al. 2012).

235 **Bioassays**

236 *Assays of immunosuppressive activity, lymphocyte viability, and antiproliferative activity against HaCaT* 237 *cells*

238 As previously reported, the immunosuppressive activities, lymphocyte viability, and antiproliferative
239 activity against HaCaT cells were evaluated using the CCK-8 method (Zhao et al. 2023, 2024).

240 In the immunosuppressive and lymphocyte viability, the primary tested concentration of all compounds
241 was 20.0 μ M, and dexamethasone (Dex) ($c = 2.0 \mu$ M) was used as a positive control. In the antiproliferative
242 activity against HaCaT cells, the primary tested concentration of all compounds was 40 μ M, and the positive
243 control was methotrexate (MTX) ($c = 40.0 \mu$ M). When the inhibition rates are greater than 50%, the IC₅₀
244 values of active compounds will be further tested and calculated. All experiments were performed in
245 triplicate.

246 *Cytokine analysis by ELISA of induced T cells*

247 The mononuclear cell suspensions (2×10^5 cells/well) were cultured with ConA (5 μ g/mL) in 96-well plates,
248 and indicated concentrations of compounds **2**, **15**, and **32** were added simultaneously. After a 48-hour culture
249 period, cytokines in the supernatants were quantified using mouse IFN- γ , IL-2, and IL-17A ELISA kits

250 (Mabtech, Sweden), following the manufacturer's protocol (Jing et al. 2021; Zhao et al. 2024).

251 ***EdU proliferation assay***

252 EdU fluorescence labeling for cell proliferation of induced T/B lymphocytes (2×10^5 cells/well) and HaCaT
253 cells (1×10^4 cells/well) of active compounds **10**, **19**, **23**, **32**, **38**, and **41** (final concentration 10 or 20 μM)
254 was performed as previously reported (Biram and Shulman 2020; Zhao et al. 2024). EdU (HF488) (the Click-
255 iTTM EdU Flow Cytometry Assay Kit, APEX BIO, USA) was added 24 h (final concentration 50 μM , T and
256 B cells) and 4 h (final concentration 10 μM , HaCaT cells) before harvesting the cells. All procedures were
257 performed according to the manufacturer's instructions for the click reaction. EdU-positive cells and
258 proliferating phase cells were analyzed with a fluorescence microscope.

259 ***Immunofluorescence protocol (cell climbing slides)***

260 The immunofluorescence protocol was performed using the reported method (Zhao et al. 2024). HaCaT cells
261 (2.0×10^5 cells/well) were plated onto 6-well plates with glass coverslips and adhered overnight (12 h) before
262 compound addition. After treatment with active compounds **10** (final concentration 31 μM) and **32** (final
263 concentration 27 μM) for 36 h, the supernatant was removed, and the cells were washed twice with PBS,
264 fixed with 4% paraformaldehyde for 15 min, and then washed with PBS three times. After blocking,
265 incubated with NF- κB p65 (p65)/phosphorylated NF- κB p65 (p-p65) antibodies, secondary antibodies
266 (Servicebio, China). Then, cells were counterstained with 4,6-diamino-2-phenylindole (DAPI) for 5 min.
267 After the PBS washing, fluorescent seal liquid was added, and the plate was monitored under an imaging
268 system (Pannoramic MIDI, 3Dhistech, Hungary). The nucleus is blue, and positive cells are green (p-p65)
269 or red (p65). The immunofluorescence areas for each indicator were analyzed in Image J.

270 ***Statistics and reproducibility***

271 GraphPad Prism 8.0 software was used for statistical data analysis, which was expressed as $\bar{X} \pm s$. One-way
272 ANOVA was used to compare the differences between groups. $P < 0.05$ or $P < 0.01$ was considered statistically
273 significant.

274 ***Ethic Statement***

275 The animal study (No. DWLL202003116) was reviewed and approved by the Animal Welfare Ethics
276 Committee of the Henan University of Chinese Medicine.

277 **Spectroscopic data of compounds**

278 ^1H , ^{13}C , 2D NMR, HRMS spectra, and computational details of compounds **1–14** were listed in the
279 [Supplementary material](#).

280 11 α ,16-Epoxy-isopimar-8(9)-en-19 β -oic acid (**1**)

281 White powders, $[\alpha]_{\text{D}}^{23} + 12.2$ (*c* 0.01, MeOH); UV (MeOH) λ_{max} (log ϵ): 201 (4.41), 214 (4.09) nm; IR
282 (MeOH) ν_{max} cm^{-1} : 3338, 2945, 1690, 2833, 1449, 1114, 1027; ^1H NMR (500 MHz CDCl_3) data see Table 1;
283 ^{13}C NMR (125 MHz CDCl_3) data see Table 1; HR-ESI-MS m/z 319.2269 $[\text{M} + \text{H}]^+$ (calcd for $\text{C}_{26}\text{H}_{31}\text{O}_3$,
284 319.2268).

285 16- α -D-Mannopyranosyloxyisopimar-8(9)-en-19-oic acid (**2**)

286 Colorless oils, $[\alpha]_{\text{D}}^{23} + 27.2$ (*c* 0.06, MeOH), UV (MeOH) λ_{max} nm (log ϵ): 201 (3.91), 241 (3.58); IR (MeOH)
287 ν_{max} cm^{-1} : 3374, 2934, 1697, 1645, 1024; ^1H NMR (500 MHz $\text{DMSO-}d_6$) data see Table 2; ^{13}C NMR (125
288 MHz $\text{DMSO-}d_6$) data see Table 2; HR-ESI-MS m/z 505.2773 $[\text{M} + \text{Na}]^+$ (calcd for $\text{C}_{26}\text{H}_{42}\text{O}_8\text{Na}$, 505.2772).

289 16- α -D-Glucopyranosyloxyisopimar-8(9)-en-19-oic acid (**3**)

290 White powders, $[\alpha]_{\text{D}}^{23} + 88.9$ (*c* 0.05, MeOH), UV (MeOH) λ_{max} nm (log ϵ): 201 (3.88), 242 (3.55); IR
291 (MeOH) ν_{max} cm^{-1} : 3288, 2933, 1696, 1457, 1034; ^1H NMR (500 MHz $\text{DMSO-}d_6$) data see Table 2; ^{13}C
292 NMR (125 MHz $\text{DMSO-}d_6$) data see Table 2; HR-ESI-MS m/z 505.2770 $[\text{M} + \text{Na}]^+$ (calcd for $\text{C}_{26}\text{H}_{42}\text{O}_8\text{Na}$,
293 505.2772)

294 Cyclo(*L*-Phe-*L*-Val-*D*-Ile-*L*-Leu-*L*-Pro) (**4**)

295 White powders, $[\alpha]_{\text{D}}^{23} - 64.4$ (*c* 0.03, MeOH), UV (MeOH) λ_{max} nm (log ϵ): 209 (3.72), 244 (3.12), 307 (2.90);
296 IR (MeOH) ν_{max} cm^{-1} : 3275, 2960, 1634, 1541, 1445; ^1H NMR (500 MHz $\text{DMSO-}d_6$) data see Table 3; ^{13}C
297 NMR (125 MHz $\text{DMSO-}d_6$) data see Table 3; HR-ESI-MS m/z : 568.3499 $[\text{M} - \text{H}]^-$ (calcd for $\text{C}_{31}\text{H}_{46}\text{O}_5\text{N}_5$,
298 568.3504).

299 Diplosporin A (**5**)

300 Yellow oils, $[\alpha]_{\text{D}}^{23} + 47.9$ (*c* 0.15, MeOH), UV (MeOH) λ_{max} nm (log ϵ): 211 (5.58), 251 (5.59); IR (MeOH)
301 ν_{max} cm^{-1} : 3396, 2937, 1660, 1611, 1456, 1106, 1032; ^1H NMR (500 MHz CDCl_3) data see Table 4; ^{13}C
302 NMR (125 MHz CDCl_3) data see Table 5; HR-ESI-MS m/z 261.1097 $[\text{M} + \text{Na}]^+$ (calcd for $\text{C}_{13}\text{H}_{18}\text{O}_4\text{Na}$,
303 261.1103).

304 Diplosporin B (**6**)

305 White powders, $[\alpha]_D^{23} + 41.3$ (*c* 1.21, MeOH), UV (MeOH) λ_{\max} nm (log ϵ): 213 (3.90), 254 (3.91); IR
 306 (MeOH) ν_{\max} cm^{-1} : 3418, 2947, 1658, 1592, 1457, 1108, 1030; ^1H NMR (500 MHz CDCl_3) data see Table
 307 4; ^{13}C NMR (125 MHz CDCl_3) data see Table 5; HR-ESI-MS m/z 261.1093 $[\text{M} + \text{Na}]^+$ (calcd for $\text{C}_{13}\text{H}_{18}\text{O}_4\text{Na}$,
 308 261.1103).

309 Diplosporin C (**7**)

310 Yellow powders, $[\alpha]_D^{23} + 11.8$ (*c* 0.37, MeOH), UV (MeOH) λ_{\max} nm (log ϵ): 222 (3.76), 245 (3.77); IR
 311 (MeOH) ν_{\max} cm^{-1} : 2934, 2876, 2828, 1660, 1620, 1435, 1088; ^1H NMR (500 MHz CDCl_3) data see Table
 312 4; ^{13}C NMR (125 MHz CDCl_3) data see Table 5; HR-ESI-MS m/z 275.1253 $[\text{M} + \text{Na}]^+$ (calcd for $\text{C}_{14}\text{H}_{20}\text{O}_4\text{Na}$,
 313 275.1259).

314 Diplosporin D (**8**)

315 Yellow oils, $[\alpha]_D^{23} - 25.6$ (*c* 0.10, MeOH), UV (MeOH) λ_{\max} nm (log ϵ): 212 (3.75), 253 (3.74); IR (MeOH)
 316 ν_{\max} cm^{-1} : 2928, 1662, 1622, 1435, 1308, 1197, 1086, 949; ^1H NMR (500 MHz CDCl_3) data see Table 4; ^{13}C
 317 NMR (125 MHz CDCl_3) data see Table 5; HR-ESI-MS m/z 253.1435 $[\text{M} + \text{H}]^+$ (calcd for $\text{C}_{14}\text{H}_{21}\text{O}_4$,
 318 253.1440).

319 Diplosporin E (**9**)

320 Yellow powders, $[\alpha]_D^{23} + 40.7$ (*c* 0.04, MeOH), UV (MeOH) λ_{\max} nm (log ϵ): 210 (3.63), 251 (3.70); IR
 321 (MeOH) ν_{\max} cm^{-1} : 3364, 2960, 1650, 1600, 1438, 1144, 1020; ^1H NMR (500 MHz CDCl_3) data see Table
 322 4; ^{13}C NMR (125 MHz CDCl_3) data see Table 5; HR-ESI-MS m/z 217.0838 $[\text{M} + \text{Na}]^+$ (calcd for $\text{C}_{11}\text{H}_{14}\text{O}_3\text{Na}$,
 323 217.0841).

324 Diplosporin F (**10**)

325 Yellow oils, UV (MeOH) λ_{\max} nm (log ϵ): 229 (3.86), 282 (3.73); IR (MeOH) ν_{\max} cm^{-1} : 1659, 1636, 1605,
 326 1451, 1202, 1114; ^1H NMR (500 MHz CDCl_3) data see Table 6; ^{13}C NMR (125 MHz CDCl_3) data see Table
 327 5; HR-ESI-MS m/z 243.0988 $[\text{M} + \text{Na}]^+$ (calcd for $\text{C}_{13}\text{H}_{16}\text{O}_3\text{Na}$, 243.0997).

328 Diplosporin G (**11**)

329 Yellow powders, UV (MeOH) λ_{\max} nm (log ϵ): 205 (3.57), 227 (3.70), 251 (3.35), 310 (3.09); IR (MeOH)
 330 ν_{\max} cm^{-1} : 2966, 2932, 1647, 1615, 1483, 11452, 1313, 1099, 828; ^1H NMR (500 MHz CDCl_3) data see
 331 Table 6; ^{13}C NMR (125 MHz CDCl_3) data see Table 5; HR-ESI-MS m/z 219.1018 $[\text{M} + \text{H}]^+$ (calcd for
 332 $\text{C}_{13}\text{H}_{15}\text{O}_3$, 219.1021).

333 Diplosporin H (**12**)

334 Yellow powders, $[\alpha]_D^{23} + 74.1$ (*c* 0.16, MeOH), UV (MeOH) λ_{\max} nm (log ϵ): 223 (3.69), 242 (3.70); IR
 335 (MeOH) ν_{\max} cm^{-1} : 1708, 1647, 1598, 1476, 1243, 1084, 1025; ^1H NMR (500 MHz CDCl_3) data see Table
 336 **6**; ^{13}C NMR (125 MHz CDCl_3) data see Table **5**; HR-ESI-MS m/z 259.0940 $[\text{M} + \text{Na}]^+$ (calcd for
 337 $\text{C}_{13}\text{H}_{16}\text{O}_4\text{Na}$, 259.0941).

338 Diplosporin I (**13**)

339 Yellow oils, $[\alpha]_D^{23} - 35.4$ (*c* 0.01, MeOH), UV (MeOH) λ_{\max} nm (log ϵ): 213 (3.74), 253 (3.74); IR (MeOH)
 340 ν_{\max} cm^{-1} : 3377, 1653, 1582, 1033, 991; ^1H NMR (500 MHz CDCl_3) data see Table **6**; ^{13}C NMR (125 MHz
 341 CDCl_3) data see Table **5**; HR-ESI-MS m/z 255.1223 $[\text{M} + \text{H}]^+$ (calcd for $\text{C}_{13}\text{H}_{19}\text{O}_5$, 255.1227).

342 (*R*)-8-methoxy-3-(methoxymethyl)isochroman-1-one (**14**)

343 White powders, $[\alpha]_D^{23} + 96.2$ (*c* 0.02, MeOH), UV (MeOH) λ_{\max} nm (log ϵ): 209 (3.72), 244 (3.12), 307
 344 (2.90); IR (MeOH) ν_{\max} cm^{-1} : 1708, 1647, 1598, 1476, 1243, 1084, 1025; ^1H NMR (500 MHz CDCl_3) data
 345 see Table **7**; ^{13}C NMR (125 MHz CDCl_3) data see Table **7**; HR-ESI-MS m/z 223.0974 $[\text{M} + \text{H}]^+$ (calcd for
 346 $\text{C}_{12}\text{H}_{15}\text{O}_4$, 223.0965).

347 **Results and Discussion**

348 *Identification of the strain*

349 The strain of *Xylaria longipes* HFG1018 was identified by employing both genetic analysis and
 350 morphological characterization. Colonies *Xylaria longipes* HFG1018 grown on OA at 25 °C for 4 weeks,
 351 with a diameter of 5 cm, white, velvety or inflorescence, appressed with entire margins; reverse white. No
 352 conidia were observed (Fig. **3**). For molecular identification, each gene sequence was analyzed using the
 353 BLAST algorithm in NCBI, and the results showed that these sequences had the highest homology to the
 354 corresponding gene sequences of *Xylaria longipes*. All the gene sequences were deposited in the GenBank
 355 database, and the corresponding accession numbers were PV523290 (ITS), MN583256 (*TUB2*), and
 356 PV558833 (*rpb2*). The ML and NJ phylogenetic trees constructed using MEGA v. 12 software indicated that
 357 isolate HFG1018 clustered with the reference strain *X. longipes* CBS 148.73 (Franco et al., 2021) (Fig. **4**).
 358 Therefore, the isolate HFG1018 in this study was confirmed as *X. longipes* through phylogenetic analysis.

359 *Structure elucidation of previously undescribed fungal metabolites (1–14)*

360 The study identified 41 secondary metabolites from the ethyl acetate (EtOAc) layers of three fermentations

361 of *X. longipes*. Among these, compounds **1–14** were found to be previously undescribed derivatives (Figs. 1
362 and 2).

363 Compound **1** was isolated as a white powder, and its molecular formula was determined to be C₂₆H₃₀O₃
364 based on HRESIMS data, showing an ion at *m/z* 319.2269 [M + H]⁺ (calculated for C₂₆H₃₁O₃, 319.2268),
365 indicating 12 degrees of unsaturation. The ¹H NMR spectrum exhibited signals for three methyl singlets (δ_{H}
366 0.85, 0.92, 1.27) and three protons attached to oxygenated carbons (δ_{H} 4.30, 3.61, 3.53) (Table 1). The ¹³C
367 NMR spectrum revealed 20 carbon signals, including three methyls (δ_{C} 18.2, 28.7, 31.8), eight sp³
368 methylenes (δ_{C} 19.3, 20.5, 32.0, 36.0, 37.8, 40.1, 40.9, 44.3), one sp³ oxygenated methylene (δ_{C} 58.5), one
369 sp³ methine (δ_{C} 53.3), one sp³ oxygenated methine (δ_{C} 66.9), three sp³ quaternary carbons (δ_{C} 27.6, 38.2,
370 43.7), a tetrasubstituted double bond (δ_{C} 133.3, 134.7), and one carbonyl (δ_{C} 181.2) (Table 1). The NMR
371 data of **1** closely resemble those of the co-isolated 16-hydroxyisopimar-7-en-19-oic acid (**15**) (Wu et al.
372 2011), suggesting that **1** is an isopimarane-type diterpenoid (Fig. 1). The presence of a carboxyl group
373 (COOH-19) and a hydroxymethyl group (CH₂O-16) was confirmed by HMBC correlations (CH₃-18 to C-
374 19) and ¹H-¹H COSY correlations (H₂-15 to H₂-16), consistent with the isopimarane family from *Xylaria*
375 species (Shiono et al. 2009; Wang et al. 2021; Zhou et al. 2021). HMBC correlations (H₃-20 to C-9) and ¹H-
376 ¹H COSY correlations (H₂-11 to H₂-12) indicated an additional hydroxy group at C-11 and a double bond at
377 C-8(9) (Fig. 5). While three rings, one carboxyl, and one double bond accounted for five degrees of
378 unsaturation, the remaining degree required an additional ring. Due to the absence of key HMBC correlations
379 from H₂-16 or H-11 to other carbons, the ring formation was deduced indirectly. Among the possible
380 positions (OH-16, OH-11, and COOH-19), COOH-19 was ruled out because of its distance from both OH-
381 16 and OH-11, as well as its typical chemical shift (δ_{C} 181.2) for a carboxyl group (Chen et al. 2020; Shiono
382 et al. 2009; Zhou et al. 2021). Thus, it was proposed that the ring form between OH-11 and OH-16. This was
383 supported by a comparison with xylarinorditerpene I, an 18-nor-isopimarane containing a cyclohexyl ether
384 between C-11 and C-13, previously isolated from the same fungus (Chen et al. 2020). The chemical shifts
385 of the oxygenated methine at C-11 [$\delta_{\text{C/H}}$ 66.9/4.30 (dd, *J* = 2.5, 2.5 Hz)] and the oxygenated methylene at C-
386 16 [$\delta_{\text{C/H}}$ 58.5/3.61 (ddd, *J* = 13.1, 11.4, 3.1 Hz); 3.53 (dd, *J* = 11.4, 5.8 Hz)] in compound **1** matched those
387 of xylarinorditerpene I [$\delta_{\text{C/H}}$ 66.4/4.34 (dd, *J* = 2.5, 2.5 Hz), -CHO-11; $\delta_{\text{C/H}}$ 58.6/3.67 (ddd, *J* = 13.2, 11.6,
388 2.9 Hz) & 3.54 (dd, *J* = 11.6, 6.1 Hz), -CH₂O-16], confirming an ether bond between C-11 and C-16 in **1**.

389 The relative configuration of **1** was determined using ROESY data (Fig. 5). The cross-peaks of H₃-18/H-
 390 5 and H₃-18/H-6 α (δ_{H} 2.00) indicated their α -orientation. In contrast, cross-peaks of H₃-20/H-11, H₃-20/H-
 391 6 β (δ_{H} 1.85), H-11/H-12 β (δ_{H} 1.71), and H-12 β /H₃-17 suggested an 11 β -H and a 17 β -CH₃. Finally, the
 392 absolute configuration and structural validity of compound **1** were confirmed by comparing experimental
 393 ECD and ¹³C NMR data with calculated spectra using Gaussian 09. The calculated results matched the
 394 experimental data (Figs. 6A and 6B), assigning **1** as 11 α ,16-epoxy-isopimar-8(9)-en-19 β -oic acid.

395 Compound **2** was isolated as colorless oils. Its molecular formula, C₂₆H₄₂O₈, matched that of co-isolate
 396 **16**, indicating six degrees of unsaturation. The ¹H NMR data of **2** (Table 2) and HSQC spectrum exhibited
 397 characteristic resonances of three methyl singlets (δ_{H} 0.85, 0.89, and 1.15). Additionally, the distinctive
 398 signal of an anomeric proton at δ_{H} 4.55 (1H, brs), alongside eight protons ranging from δ_{H} 3.28 to 3.64,
 399 suggested the presence of a hexose unit and an oxygenated methylene group. The ¹³C NMR (Table 2) and
 400 DEPT spectra confirmed the presence of 26 carbons, assigned as three methyl groups, ten methylenes (one
 401 oxygenated at δ_{C} 63.2), one methine, three sp³ quaternary carbons, two olefinic quaternary carbons (δ_{C} 124.8
 402 and 135.0), a carbonyl (δ_{C} 178.9), and six carbons from the glycosyl. Overall, the NMR data of **2** closely
 403 resembled those of 16- α -D-mannopyranosyloxyisopimar-7-en-19-oic acid (**16**) (Shiono et al. 2009). The
 404 only difference between **2** and **16** was the location of the double bond. HMBC correlation from H₃-20 to C-
 405 9 indicated that the double bond was located at C-8(9) in **2** instead of C-7(8) in **16**. The ROESY correlations
 406 of H₃-18/H-5, H₃-18/H₂-3, H₃-18/H-6 α (δ_{H} 1.85), and H₃-20/H-6 β (δ_{H} 1.72) showed that H₃-18 was α -
 407 oriented while H₃-20 was β -oriented. Moreover, ROESY correlations of H₃-17/H₂-14 (δ_{H} 1.65, 1.60) and
 408 H₂-16 β (δ_{H} 3.67)/H₂-14 α (δ_{H} 1.65) were observed, suggesting that H₃-17 was β -oriented (Fig. 5).

409 According to the literature (Shiono et al. 2009; Wang et al. 2021; Zhou et al. 2021), only two pyranoses
 410 consisting of isopimarane from the *Xylaria* species have been identified: α -D-mannose and α -D-glucose,
 411 which can be assigned easily by comparing NMR analysis. In this work, compounds **2**, **16**, and **17** were
 412 obtained simultaneously, with the weights of compound **16**, which has an α -D-mannose moiety, and
 413 compound **17**, which has an α -D-glucose moiety, being larger than that of compound **2**. Their NMR data,
 414 measured in DMSO-d₆, were carefully analyzed. The ¹³C NMR data of the pyranoses in compound **2** were
 415 nearly identical to those of compound **16**, with the largest deviation (Δ_{max}) being 0.05 ppm (C5')
 416 (Supplementary Information, Fig. S90), indicating that the pyranose in compound **2** is α -D-mannose.

417 Additionally, observed ROESY correlations of H-1'/H-2'/H-3'/H-5' and unobserved ROESY correlations of
418 H-2'/H-4' followed the configuration of α -D-mannose. Therefore, the structure of compound **2** was
419 determined as 16- α -D-mannopyranosyloxyisopimar-8(9)-en-19-oic acid.

420 Compound **3** was isolated as colorless oils. The HRESIMS spectra of compound **3** suggested a molecular
421 formula of C₂₆H₄₂O₈, identical to those of compounds **2**, **16**, and **17**. The ¹H and ¹³C NMR data of compound
422 **3** were extremely similar to those of compound **2**, except for the resonances of the glycosyl at C-1'-C-6' (**2**:
423 δ_C 99.8, 70.4, 71.1, 67.0, 74.1, 61.3; **3**: δ_C 98.6, 71.9, 73.3, 70.3, 72.8, 61.0) (Table 2). Further analysis of
424 the 2D NMR data confirmed that compounds **2** and **3** shared the same planar structure but differed in glycosyl
425 (Fig. 5). Considering the similar biosynthetic pathways, J value of H-1' (J = 3.4 Hz), ROESY correlations
426 (H-1'/H-2'/H-4'/H2-6') (Fig. 3), and comparing the chemical shifts of C-1'-C-6' of compound **3** to those of
427 compound **17** [the Δ_{\max} is 0.13 ppm (C1')] (Supplementary Information, Fig. S90), this pyranose in
428 compound **3** was deduced to be α -D-glucose. The remaining configurations of compound **3** were determined
429 to be the same as those of compound **2** due to their identical key ROESY correlations (Fig. 5). Thus, the
430 structure of compound **3** is 16- α -D-glucopyranosyloxyisopimar-8(9)-en-19-oic acid.

431 As illustrated above, compounds **2** and **3** exhibit identical planar structures and nearly identical
432 configurations, with the only difference being the orientation of the 4'-OH group in the glycosyl moiety.
433 Consequently, their circular dichroism (CD) spectra display similar trends as their calculated electronic
434 circular dichroism (ECD) spectra. Only the ECD spectrum of compound **3** was calculated and compared
435 with the experimental spectra of **2** and **3**. As shown in Fig. 6C, the diterpenoid moieties of **2** and **3** were
436 determined to have the absolute configurations 5*R*, 9*S*, 10*R*, and 13*S*.

437 Compound **4**, isolated as a colorless powder, had a molecular formula of C₃₁H₄₆O₅N₅ based on its
438 HRESIMS and comprised 14 mass units (CH₂) less than compound **18** (Wu et al. 2011). Analysis of the ¹H,
439 ¹³C, DEPT and HSQC NMR spectroscopic data of **4** (Table 3) revealed the presence of three amide protons
440 (*N*-H δ_H 7.07, 8.34, 8.35 and 8.42, respectively), six methyl groups (including five methyl singlets, and one
441 methyl triplet), six methylenes (including one *N*-methylene), eight methines (five of which are heteroatom-
442 bonded), one monosubstituted benzene, and five carboxylic carbons. Analysis of the ¹H and ¹³C NMR
443 spectroscopic data of **4** (Table 3) revealed its structural features similar to those of compound **18**, except that
444 *N*-H replaced the signals for the *N*-Me. These observations were confirmed by relevant ¹H-¹H COSY and

445 HMBC correlations (Fig. 7). By using COSY and HSQC, the independent spin systems of the type X-
446 CH(NH)-CH₂-CH₂-CH₂-X', X-CH(NH)-CH(CH₃)₂, X-CH(NH)-CH(CH₃)-CH₂-CH₃, and X-CH(NH)-CH₂-
447 CH(CH₃)₂ were identified, indicating the presence of proline, valine, isoleucine, and leucine residues. The
448 remaining independent spin system of the type X-CH(NH)-CH₂-X', together with the HMBC correlations
449 from βH (Phe) to the γ and ortho carbons of the benzene, and from H-N (δ_H 8.42) to CO (Phe), established
450 the phenylalanine (Phe) unit. Because only 10 of the calculated 11 degrees of unsaturation could be
451 accounted for, it became clear that **4** was a cyclic peptide. Upon extensive analysis of these data, compound
452 **4** was assigned as a cyclic pentapeptide containing one equivalent each of valine, leucine, isoleucine,
453 phenylalanine, and proline. The carbonyl carbons within each residue were assigned from HMBC
454 correlations between the C=O and their respective α and N protons (Table 3 and Fig. 7), which established
455 the complete amino acid sequence of **4** as cyclo-(-Phe-Pro-Leu-Ile-Val-). Since the NMR data (Table 3),
456 optical rotation (Fig. 7), and experimental CD spectrum (Supplementary Information, Fig. S100) of the **4**
457 ([α]_D²³ -64.4) were quite similar to those of **18** ([α]_D²³ -46.8) (Wu et al. 2011), indicating the L configuration
458 for Phe, Val, Ile, Leu, Pro, and D configuration for Ile.

459 Compound **5** was isolated as a yellow oil. HRMS analysis confirmed its formula as C₁₃H₁₈O₄ (indicating
460 five double bond equivalents). Analysis of the ¹H NMR spectrum of **5** (Table 4) identified 17 of the 18
461 protons, including an olefinic hydrogen (δ_H 7.99, brs), three hydrogens on oxygen carbons [δ_H 4.83 (d, J =
462 2.2 Hz), 4.31 (d, J = 13.7 Hz), 4.27 (d, J = 13.7 Hz)], five multiple protons (δ_H 1.37–2.66), a triplet methyl
463 (δ_H 1.04), and a methoxy group (δ_H 3.40). The ¹³C NMR spectrum clearly showed all 13 carbon atoms and
464 was supported by the HRMS data. Analysis of the HSQC and ¹³C NMR data (Table 5) led to the assignment
465 of two pairs of trisubstituted double bonds (δ_C 125.2, 126.0, 155.2, and 168.8), one conjugated methine (δ_C
466 179.2), four sp³ methylenes (δ_C 22.7, 25.3, 28.8, and 67.0), two sp³ methines (δ_C 42.0, 62.3), a methyl (δ_C
467 11.9), and a methoxy (δ_C 58.9). Since the 1D NMR data of **5**, including carbon types, chemical shifts, and
468 the J values were almost identical to those of (5*R*,6*R*) 6-ethyl-5-hydroxy-3-(methoxymethyl)-5,6,7,8-
469 tetrahydro-4*H*-chromen-4-one (Masahiko et al. 2014), their planar structure and relative configuration were
470 determined to be the same, which was further supported by HMBC (H₃-11 to C-6/C-10, H₃-12 to C-9, H-2
471 to C-9/C-4a/C-8a, H₂-9 to C-3/C-5, H-5 to C-3, and H-6 to C-5) and ROESY correlations (H₂-10/H-5/H-6,
472 and H₃-11/H-5) (Fig. 8). For compound **5**, the doublet of H-5 with a small J value (J = 2.2 Hz) was attributed

473 to the Jae coupling of H-5/H-6, as observed in Newman projection analysis (Fig. 8). Hence, the relative
 474 configuration of **5** is $5R^*,6R^*$. To determine the absolute configuration of **5**, the ECD trends for two possible
 475 configurations, (5*S*,6*S*)-**5** (**5a**) and (5*R*,6*R*)-**5** (**5b**), were calculated in the Gaussian 16 program
 476 (Supplementary Information). Based on the comparison of results, the ECD spectrum of **5a** matched the
 477 experimental one more closely than that of **5b** (Fig. 9). Finally, the structure of **5** was defined as (5*S*,6*S*)-6-
 478 ethyl-5-hydroxy-3-(methoxymethyl)-5,6,7,8-tetrahydro-4H-chromen-4-one and named diplosporin A.

479 Diplosporin B (**6**) was isolated as a white powder. It shares the same molecular formula ($C_{13}H_{18}O_4$) as that
 480 of **5**, based on their HRESIMS spectra. The 1D NMR data of **5** and **6** (Tables 4 and 5) were very similar,
 481 except for the resonances of CH-5 [**5**: $\delta_{C/H}$ 62.3/4.83 (d, $J = 2.2$ Hz); **6**: $\delta_{C/H}$ 69.0/4.59 (d, $J = 7.7$ Hz)]. Further
 482 analysis of the 2D NMR spectra of compound **6** (Fig. 8) indicated that it shared the same planar structure as
 483 compound **5**, while the NMR differences suggested an opposite configuration of C-5. Unlike compound **5**,
 484 the large coupling constant ($J = 7.7$ Hz) of H-5 in **6** was attributable to a J_{aa} coupling of H-5/H-6, based on
 485 Newman projection analysis (Fig. 8). Meanwhile, the ROESY correlations [H-5/H₂-10, H-5/H-7 β (δ_H 1.45),
 486 H-6/H-7 α (δ_H 2.03)] showed that H-5 and H-6 were located on opposite sides. In other words, the relative
 487 configurations of C-5 and C-6 in compound **6** were $5R^*$ and $6S^*$. To identify the absolute configuration of
 488 **6**, the ECD spectra for the two possible configurations, (5*R*,6*S*)-**6** (**6a**) and (5*S*,6*R*)-**6** (**6b**), were calculated.
 489 As shown in Fig. 9, the ECD spectrum of **6b** was more comparable to the experimental one than that of **6a**.
 490 Finally, the structure of compound **6** was defined as (5*S*,6*R*)-6-ethyl-5-hydroxy-3-(methoxymethyl)-5,6,7,8-
 491 tetrahydro-4H-chromen-4-one.

492 Diplosporin C (**7**) was isolated as a yellow powder. Its molecular formula is $C_{14}H_{20}O_4$ by HRESIMS
 493 analysis, bearing 14 mass units (CH_2) more than **5**. Moreover, the general features of its NMR data (Tables
 494 4 and 5) closely resembled those of compound **5**, indicating that they had analogous structures. Further
 495 analysis of the NMR data between compounds **5** and **7** revealed that the main difference was the presence of
 496 an additional methoxy ($\delta_{C/H}$ 60.2/3.54) for **7**, which was substituted at C-5 based on the HMBC correlation
 497 from H₃-13 to C-5 (Fig. 10). The relative configuration for compound **7** was determined by the JBCA of H-
 498 5 and ROESY analysis. The key ROESY correlations of H-6/H-5/H₂-9 and a small coupling constant ($J =$
 499 1.7 Hz) suggested that the relative configuration was the same as **5**. Finally, the absolute configuration of
 500 compound **7** was confirmed as (5*S*,6*S*) by comparing its experimental CD curve with that of compound **5**

501 (Fig. 9). Therefore, the structure of **7** was defined as (5*S*,6*S*) 6-ethyl-5-methoxy-3-(methoxymethyl)-5,6,7,8-
502 tetrahydro-4*H*-chromen-4-one.

503 Diplosporin D (**8**) had the same molecular formula as compound **7**. Furthermore, compounds **7** and **8**
504 exhibited similar signal patterns in the 1D NMR spectra (Tables 4 and 5). The primary differences between
505 **7** and **8** were the signals for CH-5 [**7**: $\delta_{\text{C/H}}$ 70.8/4.51 (d, $J = 1.7$ Hz); **8**: $\delta_{\text{C/H}}$ 73.4/4.27 (d, $J = 7.6$ Hz)] and
506 CH-6 [**7**: $\delta_{\text{C/H}}$ 41.2/1.32 (m); **8**: $\delta_{\text{C/H}}$ 36.4/1.97 (m)], suggesting that they shared the same planar structure but
507 had different relative configurations. Additionally, their CD trends were different (Fig. 9). These signals
508 indicated that the absolute configuration of compound **8** was (5*S*,6*R*). Therefore, the structure of **8** was
509 confirmed as (5*S*,6*R*) 6-ethyl-5-methoxy-3-(methoxymethyl)-5,6,7,8-tetrahydro-4*H*-chromen-4-one.

510 The molecular formula of diplosporin E (**9**) is C₁₁H₁₄O₃ according to the HRESIMS result. The ¹H NMR
511 and ¹³C NMR data (Tables 4 and 5) of **9** were similar to those of **6**, except for the presence of an additional
512 olefinic methine [$\delta_{\text{C/H}}$ 116.5/6.30 (d, $J = 5.7$ Hz)] and the absence of 3-methoxymethyl, indicating that the
513 methoxymethyl at C-3 in **6** was replaced by a proton in **9**. This modification was the reason for the doublet
514 signal of H-1 [δ_{H} 7.69 (d, $J = 5.7$ Hz)]. Furthermore, ¹H-¹H COSY and HMBC correlations (Fig. 10)
515 confirmed the planar structure as 6-ethyl-5-hydroxy-5,6,7,8-tetrahydro-4*H*-chromen-4-one. Moreover, the
516 coupling constant of H-5 ($J = 7.7$ Hz), chemical shifts of related groups (C-4a, CH-5/6, CH₂-7) (Tables 4
517 and 5), ROESY correlations (Fig. 10), and the CD spectrum for **9** (Fig. 9) closely resembled those of **6**,
518 implying that the absolute configuration of **9** is also (5*S*,6*R*).

519 Diplosporin F (**10**) was isolated as yellow oils. Its molecular formula is C₁₃H₁₆O₃, indicating six degrees
520 of unsaturation. The 1D NMR data also displayed typical signals for a 6-ethyl-3-(methoxymethyl)-4*H*-
521 chromen-4-one, similar to compounds **5** and **6**. This structural framework accounted for five of the six
522 degrees of unsaturation (Tables 4–6), while the remaining degree of unsaturation is attributed to the presence
523 of a trisubstituted double bond [$\delta_{\text{C/H}}$ 111.4/6.37 (s); 140.4]. A detailed analysis of HMBC correlations from
524 H₃-11 to C-6 and H-5 to C-4/C-8a effectively assigned the double bond between C-5 and C-6 (Fig. 11).
525 Therefore, the structure of **10** is 6-ethyl-3-(methoxymethyl)-7,8-dihydro-4*H*-chromen-4-one.

526 Diplosporin G (**11**) was obtained as a yellow powder. The molecular formula of compound **11**, C₁₃H₁₄O₃,
527 contains two mass units (H₂) less than that of **10**. The 1D NMR data of **11** were quite similar to those of **10**,
528 except for the emergence of a disubstituted double bond [$\delta_{\text{C/H}}$ 134.0/7.51 (dd, $J = 8.6, 2.2$ Hz); 118.1/7.38

529 (d, $J = 8.6$ Hz)] and the disappearance of two methines in **11** (Tables 5 and 6). Additionally, HMBC
 530 correlations from H₂-10 to C-5/C-7 indicated that this double bond was located at C7(8) (Fig. 11). This
 531 double bond, along with H-5 [δ_{H} 8.03 (d, $J = 2.2$ Hz)], formed an ABX aromatic coupling system. Therefore,
 532 the structure of **11** is 6-ethyl-3-(methoxymethyl)-4H-chromen-4-one.

533 The molecular formula of **12** is C₁₃H₁₆O₄, with six degrees of unsaturation. The similar characteristics of
 534 1D NMR data of **5** and **12** indicate they share the same scaffold. Their 1D NMR data also showed similarity
 535 to those of compound **5** (Tables 4–6). In the 1D NMR data, the signals for a terminal olefine [$\delta_{\text{C/H}}$ 138.2/6.08
 536 (m); 116.1/5.22 (dd, $J = 1.3, 1.3$ Hz), 5.19 (dd, $J = 1.3, 1.3$ Hz)] were observed instead of signals for the
 537 methyl triplet at C-11 in **12**, implying that a terminal olefine substituted the ethyl at C-6. The HMBC
 538 correlations from H-10 to C-5/C-6/C-7 and the ¹H-¹H COSY correlations of H₂-11/H-10/H-6/H-5 supported
 539 the above deduction (Fig. 11). Considering the similarities in the J value of H-5 (brs), CD spectrum (Fig. 9),
 540 and biosynthetic routes of **12** in comparison to **6**, the absolute structure of **12** was determined to be (5*S*,6*R*)-
 541 5-hydroxy-3-(methoxymethyl)-6-vinyl-5,6,7,8-tetrahydro-4H-chromen-4-one.

542 The molecular formula of diplosporin I (**13**) was determined to be C₁₃H₁₈O₅ through HRESIMS analysis,
 543 which consists of an additional oxygen atom compared to that of **6**. Additionally, the 1D NMR data (Tables
 544 4–6) showed close similarity to those of **6**, implying that **13** is a congener of **11**. The only difference between
 545 **6** and **13** is that H-6 in **6** is replaced by a hydroxy in compound **13**. Analysis of the HMBC spectrum of
 546 compound **13** enabled the above assignment (Fig. 11). Since no useful ROESY correlations were observed
 547 to confirm the relative configuration of compound **13**, calculated ¹³C NMR and ECD spectra of compound
 548 **13** were performed. There are two chiral carbons in compound **13**, so it has two pairs of possible enantiomers,
 549 (5*S**, 6*S**)-**13** and (5*S**, 6*R**)-**13**. Firstly, the ¹³C NMR data of (5*S**, 6*S**)- and (5*S**, 6*R**)-**13** were
 550 calculated using GIAO B3LYP/6-31G(d) level in Gaussian 16 and then compared with the experimental data
 551 of compound **13**. As shown in Fig. S97 (Supplementary Information), the R², MAE, and Δ_{max} of the (5*S**,
 552 6*R**)-**13** isomer [$R^2 = 0.9992$, MAE=1.6, $\Delta_{\text{max}} = 2.8$ ppm (C-12)] were better than those for the (5*S**, 6*S**)-
 553 **13** isomer [$R^2 = 0.9978$, MAE= 2.6, $\Delta_{\text{max}} = -7.1$ ppm (C-5)] (Supplementary Information), indicating the
 554 relative configuration of **13** to be (5*S**, 6*R**). Secondly, the absolute configuration of compound **13** was
 555 determined by comparing the calculated ECD with the experimental CD, showing that (5*S*, 6*R*)-**13** exhibited
 556 a similar tendency to that shown in Fig. S98 (Supplementary Information). Finally, the structure of

557 compound **13** was determined to be (5*S*,6*R*)-6-ethyl-5,6-dihydroxy-3-(methoxymethyl)-5,6,7,8-tetrahydro-
558 4*H*-chromen-4-one.

559 The molecular formula of compound **14** was determined to be C₁₂H₁₄O₄ by HRESIMS, suggesting eight
560 degrees of unsaturation. The ¹H NMR spectrum (Table 7) displayed distinguished signals for two methoxy
561 (δ_H 3.44 and 3.94), and a set of ABB' coupling benzene system [δ_H 6.82 (d, *J* = 8.0 Hz); 7.46 (dd, *J* = 8.0,
562 8.0 Hz); 6.92 (d, *J* = 8.0 Hz)]. The ¹³C NMR spectrum of **14** revealed 12 carbons, which can be assigned to
563 two methoxys (δ_C 56.3, 59.7), one sp³ methylene (δ_C 31.5), one oxygenated methylene (δ_C 73.6), one
564 oxygenated methine (δ_C 76.3), six aromatic signals (δ_C 111.1, 119.5, 134.7, 114.8, 141.7, 161.4), and one
565 ester carbonyl (δ_C 162.1) (Table 7). The NMR data of **14** resemble those of the known compound **22**
566 (Klaiklay et al. 2012), indicating that compound **14** is also an isocoumarin (Fig. 1). Further analysis of the
567 NMR data and mass spectrometry results between **14** and **22** showed that CH₃-9 in **22** was oxygenated to a
568 methoxymethyl in compound **14**, which was supported by HMBC correlation from CH₃-11 to C-9 (Fig. 11).
569 To determine the absolute configuration of the chiral carbon C-3, the ECD spectra of the two possible
570 conformers of (3*R*)-, and (3*S*)-**14** were calculated. As shown in Fig. S99 (Supplementary Information), the
571 ECD spectrum of (3*S*)-**14** matched better with the experimental one, suggesting that the absolute
572 configuration of C-3 is *S*. Therefore, the structure of **14** is (*S*)-8-methoxy-3-(methoxymethyl)isochroman-1-
573 one.

574 Besides, 27 known compounds were obtained from three fermentations of rice (**15–29**), potato-dextrose-
575 broth (PDB) (**30–34**), and glucose-peptone-yeast (GPY) (**24, 28, 35–41**). Their structures were identified by
576 comparing 1D NMR, MS, and optical data with the reported ones in the literature. As the optical value of
577 compound **26** was close to zero, it was inferred that this compound is a pair of racemates. They were
578 identified as 16-hydroxyisopimar-7-en-19-oic acid (**15**) (Wu et al. 2011), 16-*α*-*D*-
579 mannopyranosyloxyisopimar-7-en-19-oic acid (**16**) (Zhou et al. 2021; Shiono et al. 2009), 16-*α*-*D*-
580 glucopyranosyloxyisopimar-7-en-19-oic acid (**17**) (Zhou et al. 2021; Shiono et al. 2009), cyclo(N-methyl-
581 L-Phe-L-Val-D-Ile-L-Leu-L-Pro) (**18**) (Wu et al. 2011), 5-hydroxy-6-methoxy-2-methyl-4*H*-1-benzopyran-
582 4-one (**19**) (Sun et al. 2012), 5-methoxy-2-methyl-4*H*-1-benzopyran-4-one (**20**) (Teles et al. 2005), 5-
583 hydroxy-8-methoxy-2-methyl-4*H*-1-benzopyran-4-one (**21**) (Sun et al. 2012), (*S*)-8-methoxy-3-
584 methylisochroman-1-one (**22**) [[α]_D²⁵ + 211.3 (*c* 0.23, MeOH)] (Klaiklay et al. 2012), (*R*)-(-)-5-

585 methoxycarbonylmellein (**23**) $[[\alpha]_D^{23} + 118.4 (c 0.07, \text{MeOH})]$ (Gonzalez-de-Castro et al. 2014), (*S*)-5-
 586 hydroxy-8-methoxy-3-methylisochroman-1-one (**24**) $[[\alpha]_D^{23} + 126.2 (c 0.02, \text{MeOH})]$ (Harwood 1983), (*R*)-
 587 (–)-5-methoxycarbonylmellein (**25**) $[[\alpha]_D^{23} - 113.4 (c 0.03, \text{MeOH})]$ (Holker et al. 1981), (±) 8-hydroxy-4-
 588 methylisochroman-1-one (**26**) (Sumarah et al. 2011), 5-methoxy-1-naphthol (**27**) (Si et al. 2011), 1*H*-
 589 indole-3-carboxylic acid methyl ester (**28**) (Bao et al. 2007), 22,23-dihydroxyergosta-4,6,8(14)-trien-3-one
 590 (**29**) (Lee et al. 2011), (*R*)-5-carboxymellein (**30**) (Xu et al. 2020; Rukachaisirikul et al. 2009), (22*E*,24*R*)-
 591 ergosta-7,22-diene-3*β*,5*α*,6*β*-triol (**31**) (Hata et al. 2002), (3*β*,5*α*,6*β*,22*E*)-6-methoxyergosta-7,22-diene-3,5-
 592 diol (**32**) (Shimizu et al. 2016), (24*S*)-ergosta-7-ene-3*β*,5*α*,6*β*-triol (**33**) (Gao et al. 2001), 3*β*,5*α*,9*α*-
 593 trihydroxy-(22*E*,24*R*)-ergosta-7,22-dien-6-one (**34**) (Wang et al. 2017), 3-methoxy-2-phenethyl-1*H*-pyrrole-
 594 1-carbaldehyde (**35**) (Zhou et al. 2018), tryptoline (**36**) (Lu et al. 2010; Airaksinen et al. 1981), cyclo-((*S*)-
 595 Pro-(*R*)-Leu)) (**37**) (Yang et al. 2009), 1-phenylethyl-*O*-*β*-*L*-rhamnopyranoside (**38**) (Wang et al. 2014), 1-
 596 phenylethyl-*O*-*α*-*L*-rhamnopyranoside (**39**) (Chapla et al. 2018), 2-hexylidene-3-methylsuccinic acid (**40**)
 597 (Chinworrungsee et al. 2001), and 22,23-dihydroxy-ergosta-4,6,8(14)-trien-3-one-23-*β*-*D*-glucopyranoside
 598 (**41**) (Li et al. 2017).

599 The metabolites produced by *X. longipes* under three different fermentation conditions exhibit significant
 600 variation. The common compounds shared across these conditions are phenylpropanoids and ergosteroids.
 601 Phenylpropanoids, a major component of essential oils, are produced by many fungi (Chen et al. 2024).
 602 Notably, the addition of 3-methyl-2-butenol to PDB fermentation significantly increased the yield of (*R*)-5-
 603 carboxymellein (**30**) to 8.93 mg/L. Ergosteroids, integral components of the fungal cell wall, are consistently
 604 co-isolated with other metabolites.

605 Compared to liquid fermentations, rice fermentation yielded a more diverse array of metabolites, including
 606 diterpenoids, cyclic pentapeptides, 2,5-diene-4-pyrane compounds (diplosporins), phenylpropanoids, and
 607 ergosteroids. Furthermore, the metabolites from the two liquid fermentations also differed significantly. This
 608 suggests that varying fermentation conditions can induce distinct gene expressions, leading to the production
 609 of different metabolites.

610 Previous studies on *X. longipes* GPY cultures identified a series of nor-isopimarane diterpenoids (Chen et
 611 al. 2020, 2020). However, no terpenoids were detected in the liquid fermentations in this study, likely due to
 612 the addition of 5-carboxymellein, which may inhibit terpenoid synthase activity or gene expression.

613 Pimarane diterpenoids feature a 6-6-6 fused carbocyclic ring system and are classified into four subclasses:
 614 pimarane, isopimarane, ent-pimarane, and *ent*-isopimarane. While most pimarane diterpenoids are found in
 615 plants such as *Flickingeria fimbriata*, *Chloranthus henryi*, *Basilicum polystachyon*, and *Sigesbeckia*
 616 *pubescens* (Zhou et al. 2021), only a few have been identified in fungi, including *Xylaria* sp. (Chen et al.
 617 2020, 2020; Masahiko et al. 2014; Shiono et al. 2009; Wang et al. 2021; Zhou et al. 2021), *Acremonium* sp.,
 618 and *Paraconiothyrium* sp. (Ye and Ai 2022; Zhou et al. 2021).

619 In *Xylaria* sp., pimarane diterpenoids primarily belong to the isopimarane family. The first 11 α ,16-epoxy
 620 isopimarane (xylarinorditerpene K) is a norisopimarane from GPY fermentation, while 11 α ,16-epoxy-
 621 isopimar-8(9)-en-19 β -oic acid (**1**) is a rare normal isopimarane diterpenoid featuring an 11-ether substituent.
 622 Typically, isopimarane diterpenoids from *Xylaria* sp. are isolated as glycosides with a sugar moiety at C-16
 623 (Shiono et al. 2009; Wang et al. 2021; Zhou et al. 2021). To date, only two sugar moieties have been reported
 624 in these compounds: α -D-mannose and α -D-glucopyranose. Additionally, the double bond in pimarane
 625 diterpene glycosides is usually located at C-7(8) (Shiono et al. 2009; Wang et al. 2021; Zhou et al. 2021).
 626 However, in the new isopimarane glycosides **2** and **3**, the double bond is positioned at C-8(9).

627 Macrocytic peptides from *Xylaria* sp. typically consist of three to six peptides, with cyclic pentapeptides
 628 being the most common. So far, fewer than **15** such peptides have been reported from *Xylaria* sp. (Chen et
 629 al. 2024). The isolation of compound **4** contributes to the diversity of known cyclopeptides.

630 Compared to diterpenoids and macrocytic cyclic peptides, polyketides are the most abundant class of
 631 metabolites from *Xylaria* sp. In this study, 19 polyketides were isolated, including nine characterized by a 6-
 632 ethyl-4H-chromen-4-one core (diplosporins) (Ibrahim et al. 2014). Notably, nearly all reported diplosporins,
 633 including compounds **5–8** and **10–13**, feature a 3-methoxymethyl group. In contrast, compound **9** lacks this
 634 group due to degradation, making it a novel nordiplosporin.

635 **Empirical rules for the configuration of 6-ethyl-5,6,7,8-tetrahydro-4H-chromen-4-one**

636 The structural elucidation of natural products continues to pose significant challenges in chemical research.
 637 The development of advanced methodologies, including *J*-based configuration analysis (JBCA), nuclear
 638 Overhauser effect spectroscopy, quantum-chemical calculations, X-ray crystallographic analysis, and the
 639 establishment of empirical NMR data rules, has proven effective in determining both relative and absolute
 640 configurations of organic molecules. While the planar structures of most small molecules can be reliably

641 determined through NMR spectroscopy coupled with mass spectrometry, the determination of
642 stereochemical configurations remains challenging due to the structural diversity of chiral centers and the
643 difficulties in obtaining suitable single crystals for diffraction analysis. Consequently, identifying
644 characteristic NMR and/or circular dichroism (CD) patterns for specific compound classes has emerged as
645 a valuable and efficient supplementary approach for absolute configuration determination.

646 In the present study, a series of diplosporins were isolated from the rice fermentation products of *X.*
647 *longipes*. While determining their absolute configurations, distinct J-coupling constants and CD spectra
648 patterns were identified and systematically characterized. As illustrated in Figs. 8 and 9, the coupling
649 constants between H-5 and H-6 ($J_{H-5/H-6}$) provided crucial information about their spatial orientation.
650 Specifically, small coupling constants ($J < 3.0$ Hz) indicated identical orientations of H-5 and H-6, while
651 larger values suggested different orientations. Furthermore, the CD spectral patterns exhibited characteristic
652 trends: a “valley-to-peak” sequence indicated α -orientation of both H-5 and H-6, whereas the reverse pattern
653 suggested β -orientation of H-5 and α -orientation of H-6 (Fig. 9).

654 **Biological properties**

655 Building on previous reports of immunosuppressive activities of diterpenoids from *X. longipes* against the
656 proliferation of induced T and B lymphocytes, all compounds in this study were evaluated for their anti-
657 proliferative effects on ConA-induced T lymphocytes and LPS-induced B lymphocytes. As summarized in
658 Table 8, compounds 32 and 41 exhibited significant suppressive activity against ConA-induced T
659 lymphocytes, with IC_{50} values of 3.1 and 12.1 μ M, respectively. Additionally, compounds 10, 11, 32, 36, and
660 41 demonstrated inhibitory effects on LPS-induced B lymphocytes, with IC_{50} values ranging from 8.0 to
661 20.0 μ M. The positive control, Dexamethasone (Dex), showed IC_{50} values of 1.9 and 1.0 μ M, respectively.
662 Notably, all active compounds displayed CC_{50} values exceeding 20.0 μ M, indicating a superior safety profile
663 compared to Dex. In contrast, isopimarane diterpenoids 1–3 and 15–17 did not exhibit significant
664 suppressive activity against either ConA-induced T lymphocytes or LPS-induced B lymphocytes.

665 Given the reported lack of cytotoxicity of nor-isopimarane diterpenoids against T and B lymphocytes at
666 40 μ M (Chen et al., 2020), the inhibition rates of compounds 1–3 and 15–17 were further evaluated at two
667 concentrations (40.0 and 20.0 μ M). As shown in Table 9, these diterpenoids displayed dose-dependent
668 suppression of cell proliferation in both ConA-induced T lymphocytes and LPS-induced B lymphocytes,

669 with compounds **2** and **15** showing particularly notable activity. Concurrently, high cell viability (Table 9)
670 confirmed that diterpenoids **1–3** and **15–17** were non-toxic at the cellular level, further supporting their
671 safety profile.

672 Considering the notable immunosuppressive activity of compounds **2** and **32**, which possess distinct
673 structural scaffolds, their inhibitory effects were further investigated using EdU (5-ethynyl-2'-deoxyuridine)
674 imaging kits (HF488). The EdU assay, which detects proliferating cells, revealed that lymphocyte
675 proliferation (indicated by green fluorescence) was markedly enhanced in the model group (Mod) following
676 stimulation with ConA and LPS compared to the control group (Con). In contrast, treatment with compounds
677 **2** and **32** significantly suppressed the proliferation of induced T and B cells relative to the model group (Figs.
678 [12A](#) and [12B](#)).

679 Additionally, compounds **2**, **15**, and **32** were evaluated for their ability to inhibit the secretion of cytokines
680 interferon (IFN)- γ , interleukin (IL)-2, and IL-17A in mouse splenocytes, following established protocols
681 (Jing et al., 2021; Zhao et al., 2024). As illustrated in Fig. [12C](#), the levels of IFN- γ , IL-2, and IL-17A were
682 significantly elevated in the model group compared to the control group ($P < 0.0001$). Treatment with
683 compounds **2**, **15**, and **32** resulted in a significant reduction in IFN- γ secretion across all sample groups ($P <$
684 0.0001). While these compounds also decreased the secretion of IL-2 and IL-17A, most sample groups did
685 not show statistically significant differences compared to the model group. Notably, compound **15** ($40 \mu\text{M}$)
686 significantly reduced IL-2 levels ($P < 0.01$), while compounds **2** ($40 \mu\text{M}$) and **32** ($10 \mu\text{M}$) markedly lowered
687 IL-17A levels ($P < 0.05$ and $P < 0.01$, respectively). Given the established role of IFN- γ in T-cell proliferation
688 (Liu et al., 2022), the antiproliferative effects of compounds **2**, **15**, and **32** on T lymphocytes may be mediated,
689 at least in part, through the suppression of IFN- γ secretion.

690 Furthermore, all isolated compounds (**1–41**) were assessed for their antiproliferative activity against the
691 HaCaT cell line, an immortalized keratinocyte model. As summarized in Table 10, compounds **9**, **10**, **13**, **19**,
692 **22**, **24**, **25**, **28**, **30**, **32–35**, and **37–41** exhibited inhibitory effects on HaCaT cell proliferation, with IC_{50}
693 values ranging from 25.2 to 35.1 μM . Notably, the IC_{50} value of the positive control, Methotrexate (MTX),
694 was 26.4 μM . Complementary EdU experiments (Fig. [13](#)) corroborated these findings, demonstrating that
695 the proliferation rates of HaCaT cells in sample groups treated with compounds **10**, **19**, **23**, **32**, **38**, and **41**
696 were significantly reduced compared to the control group, consistent with the results obtained from the CCK-

697 8 assay.

698 Nuclear factor- κ B (NF- κ B), a family of heterodimeric proteins comprising the p50 and p65 subunits, is
699 critical in regulating cellular proliferation, differentiation, and survival (Hexum et al., 2012). Since
700 compounds **10** and **32** demonstrated inhibitory effects on the proliferation of induced T/B lymphocytes and
701 HaCaT cells, their molecular mechanisms were further investigated concerning the NF- κ B pathway. As
702 shown in Fig. 14, compounds **10** (31.0 μ M) and **32** (27.0 μ M) significantly attenuated NF- κ B activation,
703 with P values of less than 0.0001 and 0.01, respectively.

704 Psoriasis, a chronic inflammatory skin disorder affecting 2–3% of the global population, remains without
705 a definitive cure (Dai et al., 2024). The pathophysiology of psoriasis is characterized by the
706 hyperproliferation of keratinocytes, driven by excessive pro-inflammatory cytokines such as IFN- γ and IL-
707 17A, which are predominantly secreted by activated T cells, particularly Th17 cells (Castaldo et al., 2021;
708 Rendon and Schäkel, 2019). Given that compound **32** effectively suppressed the proliferation of induced T
709 lymphocytes and HaCaT cells and the secretion of key cytokines (IFN- γ and IL-17A), it emerges as a
710 promising candidate for further investigation as a potential therapeutic agent for psoriasis.

711 **Analysis of the structure-activity relationship**

712 For immunosuppressive activity, compounds **10**, **11**, **32**, **36**, and **41** demonstrated notable efficacy,
713 representing three structural classes: diplosporins (**10**, **11**), an indole alkaloid (**36**), and ergosterols (**32**, **41**).
714 Ergosterols, along with Dex, belong to the steroid family. The inhibitory effects of compounds **32** and **41** on
715 the proliferation of induced T and B lymphocytes can be attributed to their steroid nucleus. Notably, the
716 activities of compounds **32** and **41** surpassed those of their analogs **31** and **29**, respectively, suggesting that
717 the OCH₃-6 group in **32** and the 23-glucopyranosyl moiety in **41** are critical functional groups for enhancing
718 immunosuppressive activity.

719 Compounds **10**, **11**, and **36** exhibited significant selectivity in inhibiting LPS-induced B lymphocyte
720 proliferation. Among the diplosporins, the presence of a double bond at C5(6) in compounds **10** and **11**
721 appears to be a key structural feature contributing to their immunosuppressive activity. As shown in Table 8,
722 compound **10** displayed superior activity compared to compound **11**, indicating that higher degrees of
723 unsaturation may negatively impact the immunosuppressive efficacy of these compounds.

724 **Conclusion**

725 The *Xylaria* genus, a widely distributed filamentous fungus found in marine and terrestrial environments, is
 726 known for producing diverse secondary metabolites. A comprehensive phytochemical investigation of three
 727 fermentation cultures of *X. longipes* led to the isolation of 41 metabolites, including 14 novel compounds
 728 (1–14). These metabolites encompassed a variety of structural classes, such as isopimarane-type diterpenoids,
 729 isopimarane-type diterpenoid glycosides, cyclic peptides, polyketides, phenylpropanoids, pyrroles, and
 730 ergosterols. Notably, a shift in the production of secondary metabolites was observed when transitioning
 731 from solid (rice) to liquid media (PDB and GPY, both supplemented with 3-methyl-2-butenol), highlighting
 732 the media-dependent nature of metabolite biosynthesis. This study also validated the utility of combining ³J
 733 coupling constants with circular dichroism (CD) trends for determining the absolute configurations of C-5
 734 and C-6 in diplosporins.

735 All isolated compounds were evaluated for their anti-proliferative activity against ConA-induced T
 736 lymphocytes, LPS-induced B lymphocytes, and HaCaT cells *in vitro*, with several compounds demonstrating
 737 significant activity. Ergosteroids **32** and **41** exhibited potent immunosuppressive and antiproliferative effects
 738 against HaCaT cells while maintaining high lymphocyte safety. Cytokine analysis revealed that active
 739 compounds **2**, **15**, and **32** significantly reduced IFN- γ levels, with compound **32** (10 μ M) also inhibiting IL-
 740 17A secretion. Further immunofluorescence assays indicated that the antiproliferative effects of compounds
 741 **10** and **32** on HaCaT cells were mediated, at least in part, through the inactivation of NF- κ B via reduced
 742 phosphorylation of p65. Given its multifaceted activities, compound **32** is a promising candidate for
 743 developing therapeutic agents for psoriasis.

744 **Supplementary Information**

745 The online version contains supplementary material available at <https://doi.org/XXX>, including the NMR, HRMS data,
 746 computational details, and other relevant information on compounds 1–14, together with all the obtained sequences deposited
 747 in GenBank.

748 **Adherence to national and international regulations**

749 Not applicable.

750 **Authors' contributions**

751 ZZZ, XP, and WSF conceived and designed the experiments. YW, LLW, and MJS performed all experiments and contributed
 752 to the data acquisition. XYW, JKW, ZZW, and YW performed all data analyses. ZZZ wrote the original manuscript. All authors
 753 reviewed and improved the manuscript and have agreed to the published version of the manuscript.

754 **Funding**

755 This work was supported by the National Natural Science Foundation of China (82003607, 82274114), the Excellent Young
756 Scientists Fund of the Natural Science Foundation of Henan Province (242300421091), Natural Science Foundation of Henan
757 (CN) (232301420094), Henan Postdoctoral Research Foundation (CN) (HN2022078), Scientific and Technological Key
758 Project in Henan Province (CN) (242102310567, 242102311289), Science and Technology Innovative Research Team in
759 Higher Educational Institutions of Henan Province (CN) (24IRTSTHN039), Scientific Research Nursery Project of Henan
760 University of Chinese Medicine (CN) (MP2024-10).

761 **Availability of data and materials**

762 Not applicable.

763 **Declarations**

764 **Ethics approval and consent to participate**

765 The animal study (No. DWLL202003116) was reviewed and approved by the Animal Welfare Ethics Committee of the Henan
766 University of Chinese Medicine.

767 **Consent for publication**

768 Not applicable.

769 **Competing interests**

770 The authors declare that they have no competing interests.

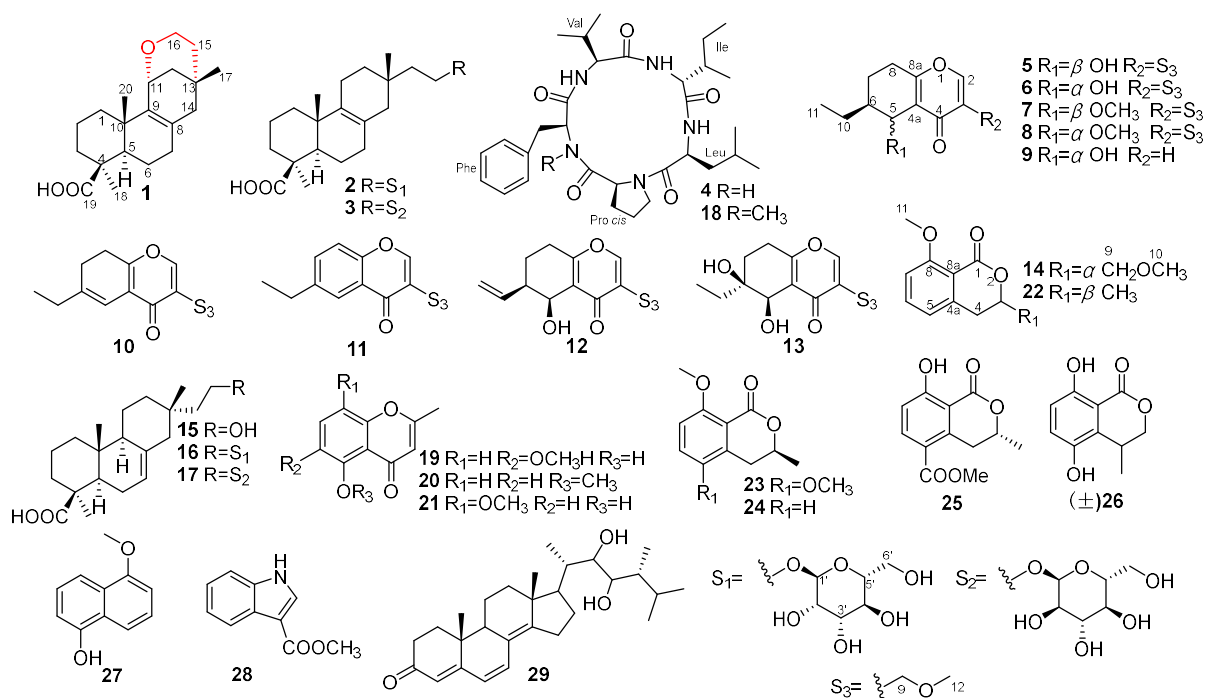
771 **References**

- 772 Airaksinen MM, Kari I (1981) β -carbolines, psychoactive compounds in the mammalian body. Part I: Occurrence, origin and
773 metabolism. *Med Biol* 59(1):21–34.
- 774 Bao B, Zhang P, Lee Y, et al (2007) Monoindole alkaloids from a marine sponge *Spongosorites* sp. *Mar Drugs* 5(2):31–39.
775 <https://doi.10.3390/md502031>
- 776 Biram A, Shulman Z (2020). Evaluation of B Cell proliferation *in vivo* by EdU incorporation assay. *Bio Protoc* 10: e3602.
777 <https://doi.10.21769/BioProtoc.3602>
- 778 Bode HB, Bethe B, Höfs R, Zeeck A (2002) Big effects from small changes: possible ways to explore nature's chemical
779 diversity. *Chembiochem* 3(7):619–27. [https://doi.10.1002/1439-7633\(20020703\)3:7<619::AID-CBIC619>3.0.CO;2-9](https://doi.10.1002/1439-7633(20020703)3:7<619::AID-CBIC619>3.0.CO;2-9)
- 780 Bruhn T, Schaumlöffel A, Hemberger Y, Bringmann G (2012) Spec Dis, version 1.71, University of Würzburg, Germany.
- 781 Castaldo G, Pagano I, Grimaldi M et al (2021) Effect of very-low-calorie ketogenic diet on psoriasis patients: A nuclear
782 magnetic resonance-based metabolomic study. *J Proteome Res* 20(3):1509–1521.
783 <https://doi.10.1021/acs.jproteome.0c00646>
- 784 Chapla VM, Zeraik ML, Cafeu MC et al (2018) Griseofulvin, diketopiperazines and cytochalasins from endophytic fungi
785 *Colletotrichum crassipes* and *Xylaria* sp., and their antifungal, antioxidant and anticholinesterase activities. *J Brazil Chem*
786 *Soc* 29(8):1707–1713. <https://doi.10.21577/0103-5053.20180045>
- 787 Chen HP, Li J, Zhao ZZ et al (2020) Diterpenes with bicyclo[2.2.2]octane moieties from the fungicolous fungus *Xylaria*
788 *longipes* HFG1018. *Org Biomol Chem* 18(13):2410–2415. <https://doi.10.1039/d0ob00220h>
- 789 Chen HP, Zhao ZZ, Cheng GG et al (2020) Immunosuppressive nor-isopimarane diterpenes from cultures of the fungicolous
790 fungus *Xylaria longipes* HFG1018. *J Nat Prod* 83(2):401–412. <https://doi.org/10.1021/acs.jnatprod.9b00889>
- 791 Chen W, Yu M, Chen S et al (2024) Structures and biological activities of secondary metabolites from *Xylaria* spp. *J Fungi*
792 10(3):190. <https://doi.10.3390/jof10030190>
- 793 Chinworrungsee M, Kittakoop P, Isaka M et al (2001) Antimalarial halorosellinic acid from the marine fungus *Halorosellinia*

- 794 *oceanica*. Bioorg Med Chem Lett 11(15):1965–1969. [https://doi.10.1016/s0960-894x\(01\)00327-4](https://doi.10.1016/s0960-894x(01)00327-4)
- 795 Dai X, Permana AD, Li M et al (2024) Calcipotriol nanosuspension-loaded trilayer dissolving microneedle patches for the
796 treatment of psoriasis: *In vitro* delivery and *in vivo* antipsoriatic activity studies. Mol Pharm 21(6):2813–2827.
797 <https://doi.10.1021/acs.molpharmaceut.3c01223>
- 798 Franco MEE, Wisecaver JH, Arnold AE, Ju YM, Slot JC, Ahrendt S, Moore LP, Eastman KE, Scott K, Konkel Z, Mondo SJ,
799 Kuo A, Hayes RD, Haridas S, Andreopoulos B, Riley R, LaButti K, Pangilinan J, Lipzen A, Amirebrahimi M, Yan J,
800 Adam C, Keymanesh K, Ng V, Louie K, Northen T, Drula E, Henrissat B, Hsieh HM, Youens-Clark K, Lutzoni F,
801 Miadlikowska J, Eastwood DC, Hamelin RC, Grigoriev IV, U'Ren JM (2022) Ecological generalism drives hyperdiversity
802 of secondary metabolite gene clusters in xylarialean endophytes. New Phytol 233(3):1317–1330. [https://doi.](https://doi.10.1111/nph.17873)
803 [10.1111/nph.17873](https://doi.10.1111/nph.17873).
- 804 Frisch MJ, Trucks GW, Schlegel HB et al (2016) Gaussian, Inc., Wallingford CT.
- 805 Gao JM, Dong ZJ, Liu JK (2001). A new ceramide from the basidiomycete *Russula cyanoxantha*. Lipids 36(2):175–181.
806 <https://doi.10.1007/s11745-001-0704-x>
- 807 Gonzalez-de-Castro A, Robertson CM, Xiao J (2014) Dehydrogenative α -oxygenation of ethers with an iron catalyst. J Am
808 Chem Soc 136(23):8350–8360. <https://doi.10.1021/ja502167h>
- 809 Harwood LM (1983) An investigation into the regioselectivity of the acid catalysed Claisen rearrangement of methyl 4-and 5-
810 allyloxy-2-hydroxybenzoate and derivatives. J Am Chem Soc Chem Commun (9):530–532.
811 <https://doi.10.1039/C39830000530>
- 812 Hata K, Sugawara F, Ohisa N, et al (2002) Stimulative effects of (22*E*,24*R*)-ergosta-7,22-diene-3 β ,5 α ,6 β -triol from fruiting
813 bodies of *Tricholoma auratum*, on a mouse osteoblastic cell line, MC3T3-E1. Biol Pharm Bull 25(8):1040–1044.
814 <https://doi.10.1248/bpb.25.1040>
- 815 Hexum JK, Tello-Aburto R, Struntz NB et al (2012) Bicyclic cyclohexenones as inhibitors of NF- κ B signaling. ACS Med
816 Chem Lett 3:459–464. <https://doi.10.1021/ml300034a>
- 817 Holker JSE, Simpson TJ (1981) Studies on fungal metabolites. Part 2. Carbon-13 nuclear magnetic resonance biosynthetic
818 studies on pentaketide metabolites of *Aspergillus melleus*: 3-(1,2-epoxypropyl)-5,6-dihydro-5-hydroxy-6-methylpyran-
819 2-one and mullein. J Am Chem Soc Perkin Transactions 1:1397–1400.
- 820 Ibrahim A, Sørensen D, Jenkins HA et al (2014) New diplosporin and agistatine derivatives produced by the fungal endophyte
821 *Xylaria* sp. isolated from *Vitis labrusca*. Phytochemistry Lett 9:179–183. <http://dx.doi.org/10.1016/j.phytol.2014.06.011>
- 822 Jing SX, Fu R, Li CH et al (2021) Immunosuppressive sesterterpenoids and norsesterterpenoids from *Colquhounia coccinea*
823 var. *mollis*. J Org Chem 86: 11169–11176. <https://doi.10.1021/acs.joc.1c00374>
- 824 Klaiklay S, Rukachaisirikul V, Sukpondma Y et al (2012) Metabolites from the mangrove-derived fungus *Xylaria cubensis*
825 PSU-MA34. Arch Pharm Res 35(7):1127–1131. <https://doi.10.1007/s12272-012-0701-y>
- 826 Lee IS, Kim JP, Na MK et al (2011) Cytotoxicity of ergosterol derivatives from the fruiting bodies of *Hygrophorus russula*.
827 Nat Prod Sci 17(2):85–89.
- 828 Li W, Yang XQ, Yang YB et al (2017) A novel steroid derivative and a new steroidal saponin from endophytic fungus *Xylaria*
829 sp. Nat Prod Commun 12(6):901–904.
- 830 Li YY, Hu ZY, Shen YM (2011) Two new cyclopeptides and one new nonenolide from *Xylaria* sp. 101. Nat Prod Commun
831 6(12):1843–1846.
- 832 Liu W, Zhang S, Wang (2022) J IFN- γ , should not be ignored in SLE. Front Immunol 13: 954706.
833 <https://doi.10.3389/fimmu.2022.954706>
- 834 Lu YN, Pan CQ, Xi DY et al (2010) Alkaloids from the sea anemone *Haliplanella luciae*. Chin J Mar Drugs 29(1):45–49.
835 <https://doi.10.3724/SP.J.1231.2010.06703>

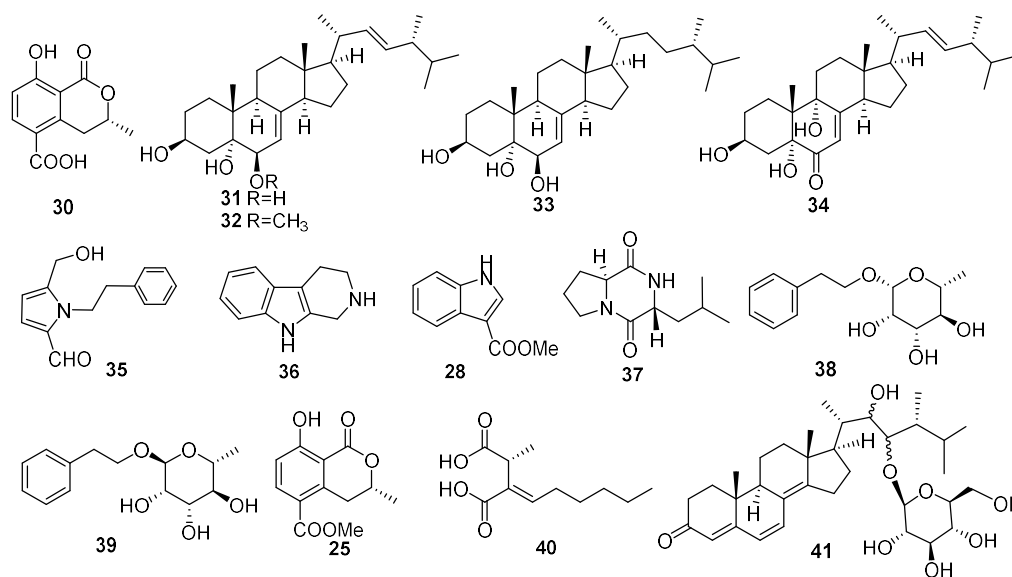
- 836 Masahiko I, Arunrat Y, Sumalee S et al (2014) Isopimaranes and eremophilanes from the wood-decay fungus *Xylaria*
837 *allantoidea* BCC 23163. *Phytochemistry Lett* 8:59–64. <http://dx.doi.org/10.1016/j.phytol.2014.06.011>
- 838 Pan R, Bai X, Chen J et al (2019) Exploring structural diversity of microbe secondary metabolites using OSMAC strategy: A
839 literature review. *Front Microbiol* 10:294. <https://doi.10.3389/fmicb.2019.00294>
- 840 Pfützte S, Charria-Girón E, Schulzke E et al (2024) Depicting the chemical diversity of bioactive meroterpenoids produced by
841 the largest organism on earth. *Angew Chem Int Ed Engl.* 63(16):e202318505. <https://doi.10.1002/anie.202318505>
- 842 Rendon A, Schäkel K (2019) Psoriasis pathogenesis and treatment. *Int J Mol Sci* 20:1475.
843 <https://doi.org/10.3390/ijms20061475>
- 844 Rukachaisirikul V, Khamthong N, Sukpondma Y et al (2009) An [11]cytochalasin derivative from the marine-derived fungus
845 *Xylaria* sp. PSU-F100. *Chem Pharm Bull (Tokyo)* 57(12):1409–1411. <https://doi.10.1248/cpb.57.1409>
- 846 Shimizu T, Kawai J, Ouchi K et al (2016) Agarol, an ergosterol derivative from *Agaricus blazei*, induces caspase-independent
847 apoptosis in human cancer cells. *Int J Oncol* 48(4):1670–1678. <https://doi.10.3892/ijo.2016.3391>
- 848 Shiono Y, Motoki S, Koseki T et al (2009) Isopimarane diterpene glycosides, apoptosis inducers, obtained from fruiting bodies
849 of the ascomycete *Xylaria polymorpha*. *Phytochemistry* 70(7):935–939. <https://doi.10.1016/j.phytochem.2009.03.023>
- 850 Si CL, Zhang Y, Zhu ZY et al (2011) Chemical constituents with antioxidant activity from the pericarps of *Juglans sigillata*.
851 *Chem Nat Compd* 47:442–445. <https://doi.10.1007/s10600-011-9956-7>
- 852 Sumarah MW, Puniani E, Blackwell BA, Miller JD (2008). Characterization of polyketide metabolites from foliar endophytes
853 of *Picea glauca*. *J Nat Prod* 71(8):1393–1398. <https://doi.10.1021/np800192f>
- 854 Sun JZ, Liu XZ, Mckenzie EHC et al (2019) Fungicolous fungi: Terminology, diversity, distribution, evolution, and species
855 checklist. *Fungal Divers* 95:337–430. <https://doi.10.1007/s13225-019-00422-9>
- 856 Sun YW, Liu GM, Huang H, Yu PZ (2012) Chromone derivatives from *Halenia elliptica* and their anti-HBV activities.
857 *Phytochemistry* 75:169–176. <https://doi.10.1016/j.phytochem.2011.09.015>
- 858 Teles HL, Silva GH, Castro-Gamboa I et al (2005) Benzopyrans from *Curvularia* sp., an endophytic fungus associated with
859 *Ocotea corymbosa* (Lauraceae). *Phytochemistry* 66(19):2363–2367. <https://doi.10.1016/j.phytochem.2005.04.043>
- 860 Wang F, Han S, Hu S et al (2014) Two new secondary metabolites from *Xylaria* sp. cfcc 87468. *Molecules* 19(1):1250–1257.
861 <https://doi.10.3390/molecules19011250>
- 862 Wang J, Zhang Z, Wang Y et al (2017) Chemical constituents from mycelia and spores of fungus *Cordyceps cicadae*. *Chin*
863 *Herb Med* 9(2):188–192. [https://doi.10.1016/S1674-6384\(17\)60094-7](https://doi.10.1016/S1674-6384(17)60094-7)
- 864 Wang QY, Chen HP, Liu JK (2021) Isopimarane diterpenes from the rice fermentation of the fungicolous fungus *Xylaria*
865 *longipes* hfg1018. *Phytochemistry Lett* 45:100–104. <https://doi.org/10.1016/j.phytol.2021.08.005>
- 866 Wu W, Dai H, Bao L et al (2011) Isolation and structural elucidation of proline-containing cyclopentapeptides from an
867 endolichenic *Xylaria* sp. *J Nat Prod* 74(5):1303–1308. <https://doi.10.1021/np100909y>
- 868 Xu ZL, Zheng N, Cao S, et al (2020) Secondary metabolites from the endophytic fungus *Stemphylium lycopersici* and their
869 antibacterial activities. *Chem Nat Compd* 56(6):1162–1165. <https://doi.10.1007/s10600-020-03256-z>
- 870 Yang B, Dong J, Zhou X et al (2009) Proline-containing dipeptides from a marine sponge of a *Callyspongia* Species. *Helvetica*
871 *Chimica Acta* 92(6):1112–1117. <https://doi.10.1002/hlca.200800422>
- 872 Ye K, Ai HL (2022) Pimarane diterpenes from fungi. *Pharmaceuticals (Basel)* 15(10):1291. <https://doi.10.3390/ph15101291>.
873 <https://doi.10.3390/ph15101291>
- 874 Zhang H, Deng Z, Guo Z et al (2015) Effect of Culture Conditions on Metabolite Production of *Xylaria* sp. *Molecules*
875 20(5):7940–50. <https://doi.10.3390/molecules20057940>
- 876 Zhang D, Gao F, Jakovlić I, Zou H, Zhang J, Li WX, Wang GT (2020) PhyloSuite: An integrated and scalable desktop platform
877 for streamlined molecular sequence data management and evolutionary phylogenetics studies. *Mol Ecol Resour* 20(1):

- 878 348-355. <https://doi.org/10.1111/1755-0998>.
- 879 Zhao ZZ, Liang XB, He HJ et al (2024) Diterpenoids with potent anti-psoriasis activity from *Euphorbia helioscopia* L.
- 880 Molecules 29(17): 4104. <https://doi.org/10.3390/molecules29174104>
- 881 Zhao ZZ, Zhang F, Ji BY et al (2023). Pyrrole alkaloids from the fruiting bodies of edible mushroom *Lentinula edodes*. RSC
- 882 adv 13:18223–18228. <https://doi.org/10.1039/d3ra02672h>
- 883 Zhou P, Zheng M, Li XN et al (2021) Hypoxylonoids A-G: Isopimarane diterpene glycosides from *Xylaria hypoxylon*.
- 884 Phytochemistry 182:112613. <https://doi.org/10.1016/j.phytochem.2020.112613>
- 885 Zhou M, Zhang RQ, Chen YJ et al (2018) Three new pyrrole alkaloids from the roots of *Lepidium meyenii*. Phytochem Lett
- 886 23:137–140. <https://doi.org/10.1016/j.phytol.2017.12.002>
- 887



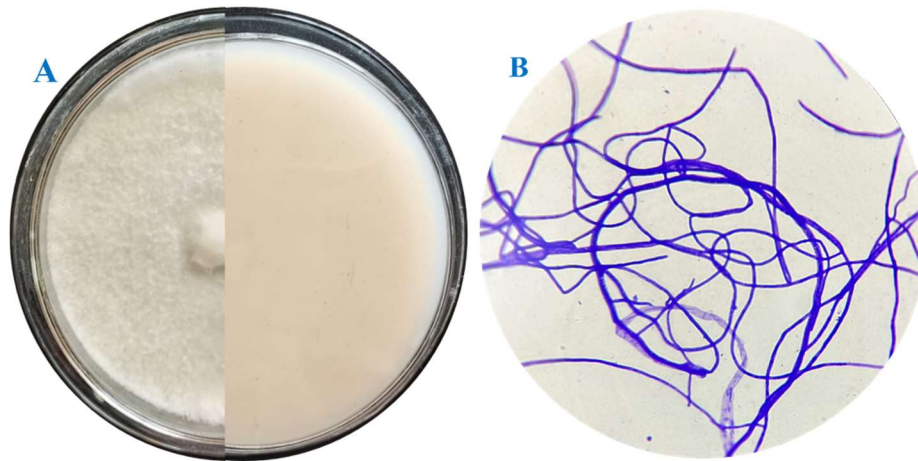
888
889

Fig. 1 The structures of compounds **1–29** from the rice fermentation of *X. longipes* HFG1018.

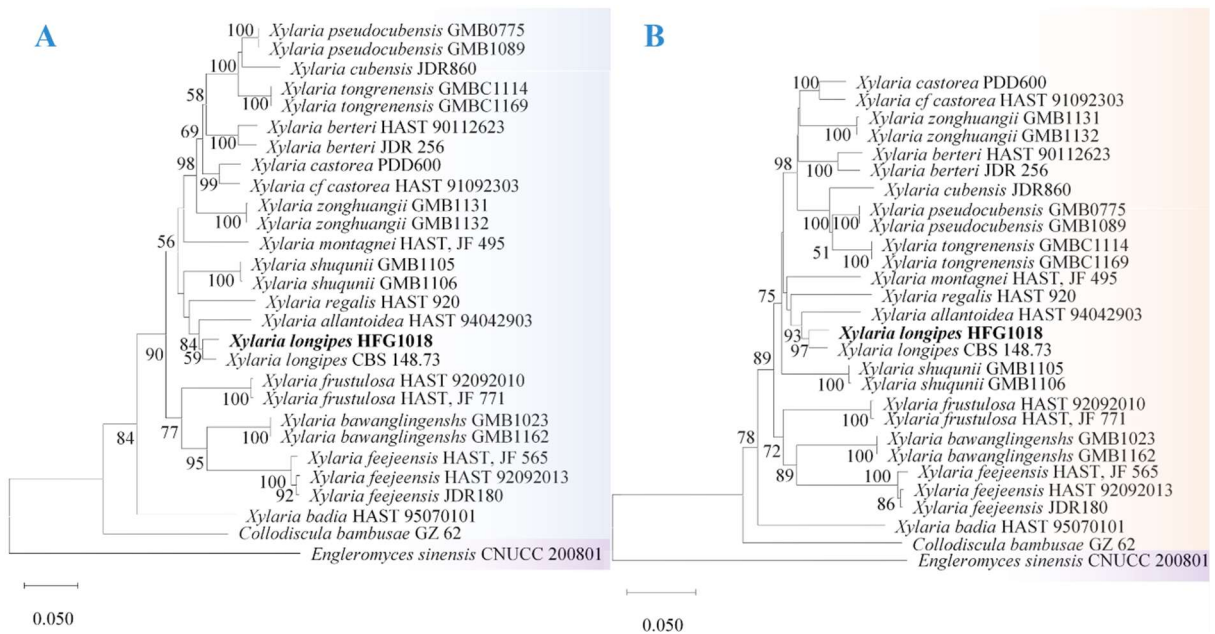


890
891
892
893

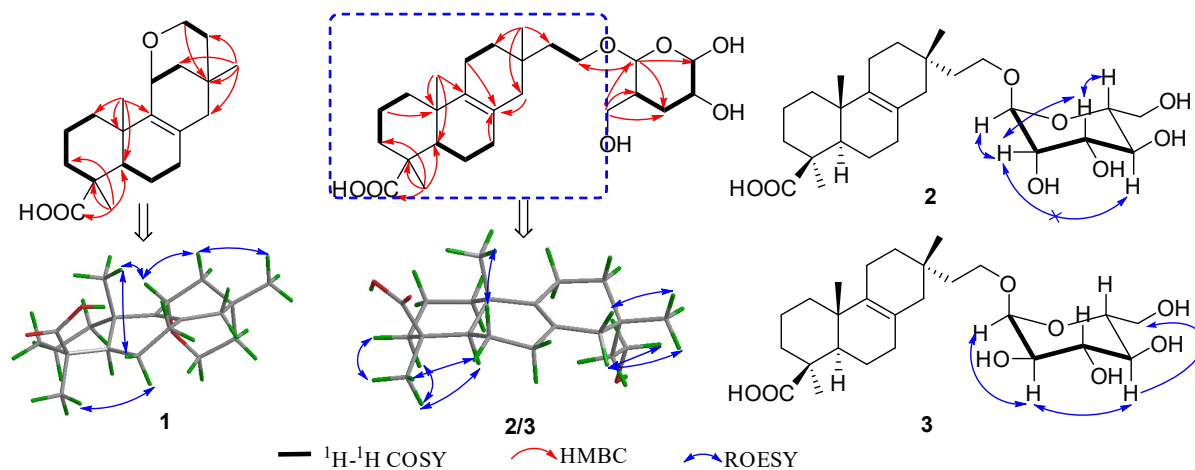
Fig. 2 The structures of compounds **30–34** (PDB) and **35–41** (GPY) from liquid fermentations of *X. longipes* HFG1018.



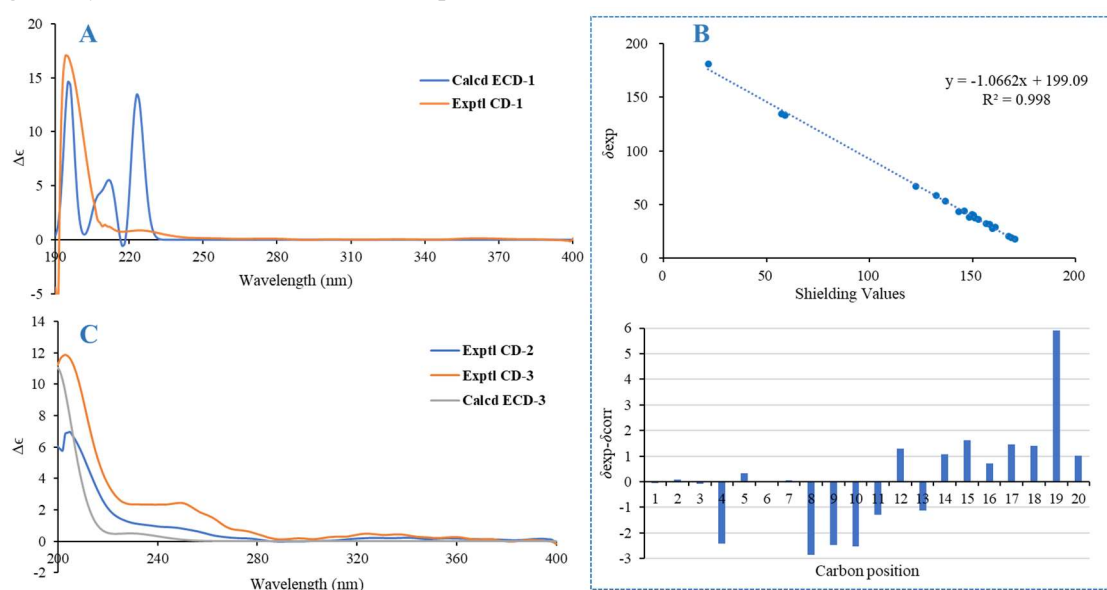
894
 895 **Fig. 3** The phenotypal and morphological characters of *Xylaria longipes* HFG1018. (A) The colony. (B)
 896 Methylene blue-stained Mycelium (100 ×).



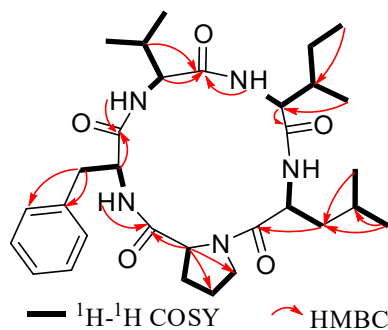
897
 898 **Fig. 4** Maximum likelihood trees of *Xylaria* constructed using internal transcribed spacer (ITS), β -tubulin
 899 gene (TUB2), and DNA-directed RNA Polymerase II subunit 2 (rpb2) gene sequence data sets. Bootstrap
 900 support values of maximum likelihood (MLBP) above 50% are shown at the nodes. The tree was rooted to
 901 *Engleromyces sinensis* CNUCC 200801. The strain *Xylaria longipes* described species are marked in bold.
 902 (A) ML tree. (B) NJ tree.
 903



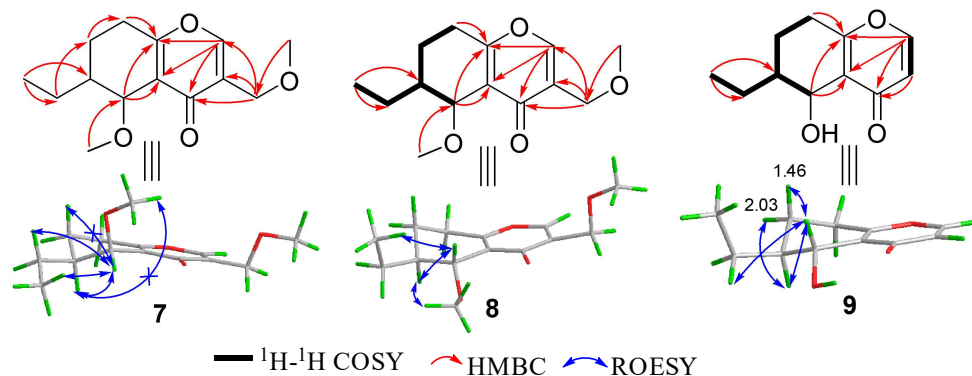
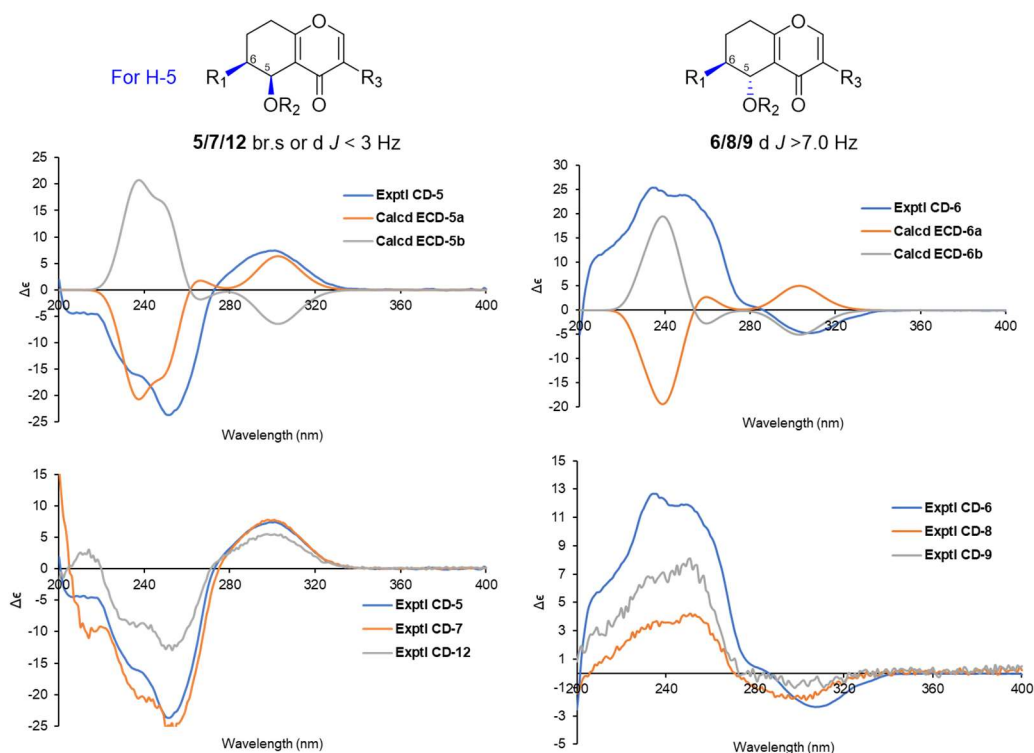
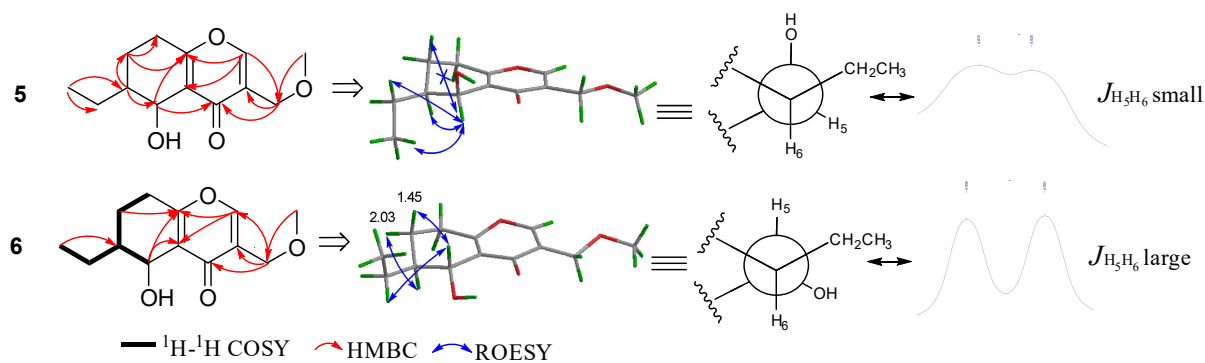
904
905 **Fig. 5** Key 2D NMR correlations of compounds 1–3.

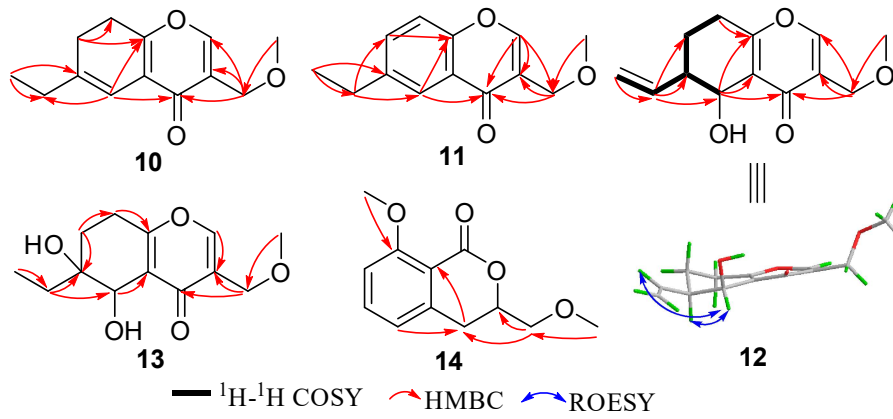


906
907 **Fig. 6** (A) Comparison of the calculated ECD spectrum for **1** ($\sigma = 0.10$ eV, and UV shift 5 nm) with its
908 experimental CD spectrum in MeOH; (B) Comparison of the calculated ^{13}C NMR data for **1** with its
909 experimental spectrum in CDCl_3 ; (C) Comparison of the calculated ECD spectrum for **2, 3** ($\sigma = 0.30$ eV, and
910 UV shift 7 nm) with their experimental CD spectra in MeOH.



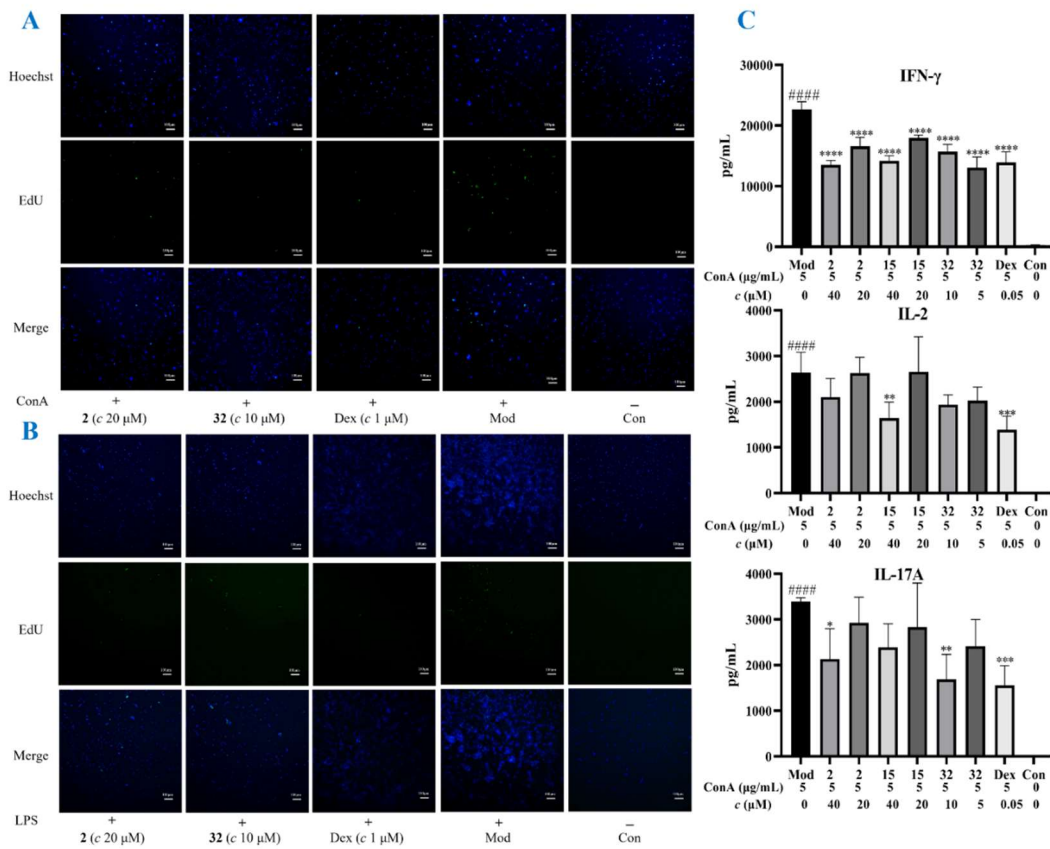
911
912 **Fig. 7** Key HMBC correlations of compound **4**.





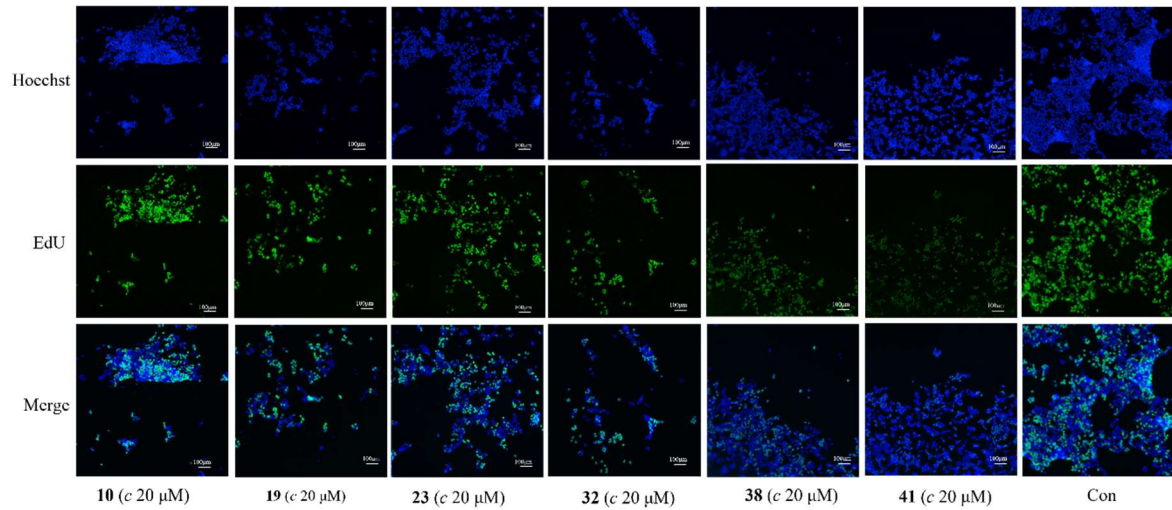
922

923 **Fig. 11** Key 2D NMR correlations of compounds 10–14.



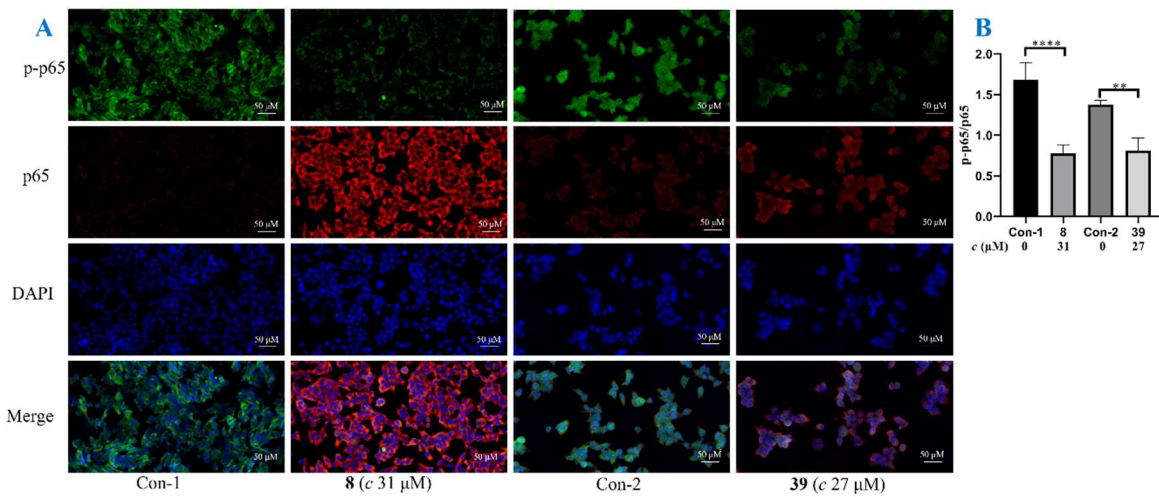
924

925 **Fig. 12** (A/B) Inhibitory activities of compounds 2 ($c = 20 \mu\text{M}$), 32 ($c = 10 \mu\text{M}$), and Dex ($c = 2, 1 \mu\text{M}$) against
 926 induced T cells (Con A $5 \mu\text{g/mL}$) and B (LPS $15 \mu\text{g/mL}$) cells measured by EdU. (C) Concentrations of IFN- γ ,
 927 IL-2, and IL-17A of induced T cells (Con A $5 \mu\text{g/mL}$) in different groups (vs Con ##### $P < 0.0001$; vs Mod,
 928 **** $P < 0.0001$, ** $P < 0.01$, * $P < 0.05$).



929
930
931

Fig. 13 Inhibitory activities of compounds **10**, **19**, **23**, **32**, **38**, and **41** ($c = 20 \mu\text{M}$), against HaCaT cells measured by EdU.



932
933
934
935
936

Fig. 14 (A) Immunofluorescence images: Effects of compounds **10** ($c = 31 \mu\text{M}$) and **32** ($c = 27 \mu\text{M}$) on p-p65 and p65 expression levels in HaCaT cells. (B) Ratios of p-p65/p65 of HaCaT cells in different groups (vs Con, **** $P < 0.0001$, ** $P < 0.01$).

937

938 **Table 1** ^1H (500 MHz) and ^{13}C NMR (125 MHz) data of compound **1** (CDCl_3)

No.	δ_{C}	δ_{H}
1	36.0	2.23, m; 1.84*
2	19.3	1.84*; 1.52, m
3	37.8	2.19, br.d (13.9); 1.04, ddd (13.9, 13.9, 4.5)
4	43.7	
5	53.3	1.40, d (12.2)
6	20.5	2.00, m; 1.85, m
7	32.0	2.10, m; 1.90, m
8	134.7	
9	133.3	
10	38.2	
11	66.9	4.30, dd (2.5, 2.5)
12	40.1	1.71, dd (11.6, 3.5); 1.30, dd (11.6, 3.5)
13	27.6	
14	44.3	1.81, m, 2H
15	40.9	1.50, m; 1.19, m
16	58.5	3.61, ddd (13.1, 11.4, 3.1); 3.53, dd (11.4, 5.8)
17	31.8	0.92, s
18	28.7	1.27, s
19	181.2	
20	18.2	0.85, s

* overlapped

939

940 **Table 2** ^1H (500 MHz) and ^{13}C NMR (125 MHz) data of compounds **2** and **3** (DMSO- d_6 , J in Hz)

No.	2		3	
	δ_{C}	δ_{H}	δ_{C}	δ_{H}
1	36.7	1.75, m; 1.01, m	36.6	1.75, m; 1.03, m
2	19.3	1.74, m; 1.42, m	19.3	1.76 *, 1.41, m
3	37.3	2.02, m; 0.97, m	37.3	2.03, m; 0.99, m
4	42.9		42.9	
5	52.6	1.29, d (11.8)	52.6	1.29, d (11.5)
6	20.5	1.85 *, 1.72, m	20.5	1.86 *, 1.72, m
7	32.8	1.85*; 1.80, m	32.8	1.86 *, 1.81, m
8	124.8		124.8	
9	135.0		135.0	
10	37.7		37.7	
11	20.3	1.90, m; 1.83, m	20.4	1.90, m; 1.83, m
12	34.1	1.44, m; 1.17, m	34.0	1.45, m; 1.16, m
13	30.2		30.0	
14	43.8	1.65, d (17.9); 1.60 d (17.9)	43.9	1.65, d (18.0); 1.60 d (18.0)
15	36.2	1.47, m; 1.34, m	36.4	1.49, m; 1.36, m
16	63.2	3.67*; 3.32*	63.6	3.65, m; 3.32, m
17	27.2	0.89, s	27.2	0.87, s
18	28.3	1.15, s	28.3	1.13, s
19	178.9		178.6	
20	17.5	0.85, s	17.5	0.84, s
1'	99.8	4.55, brs	98.6	4.58, d (3.4)
2'	70.4	3.55, brs	71.9	3.16, dd (9.3, 3.4)
3'	71.1	3.43*	73.3	3.37, t (9.3)
4'	67.0	3.36, t (9.3)	70.3	3.05, t (9.3)
5'	74.1	3.28, m	72.8	3.33*
6'	61.3	3.64, dd (11.6, 2.1); 3.44, dd (11.6, 6.3)	61.0	3.60, brd (11.4); 3.43, dd (11.6, 3.0)

* overlapped

941

942

943 **Table 3** ^1H (500 MHz) and ^{13}C NMR (125 MHz) data of compound **4** (DMSO- d_6 , J in Hz)

Amino acid	No.	δ_{C}	δ_{H}
<i>L</i> -phenylalanine	CO	171.4	
	α	54.2	4.37, dd (15.5, 7.9)
	β	36.6	2.84, m
	γ	137.5	
	<i>ortho</i>	129.2	7.17, m
	<i>meta</i>	128.0	7.24, m
	<i>para</i>	126.2	7.24, m
	NH		8.42, d (7.9)
<i>L</i> -valine	CO	170.5	
	α	58.2	3.83, t (9.2)
	β	26.1	1.94, m
	γ	19.7	0.81, d (6.2)
		18.4	0.62, d (6.6)
	NH		8.35, d (9.2)
<i>D</i> -isoleucine	CO	170.2	
	α	55.7	4.19, dd (8.5, 7.1)
	β	37.8	1.52, m
	γ	25.6	1.27, m; 1.01, m
	σ	11.5	0.83, d (6.2)
	β -CH ₃	14.4	0.72, d (6.9)
	NH		7.07, d (8.5)
<i>L</i> -leucine	CO	168.8	
	α	47.6	4.61, dd (14.5, 8.6)
	β	41.5	1.51, m; 1.41, m
	γ	24.4	1.35, m
	σ	22.7	0.84, d (6.3)
		22.4	0.84, d (6.2)
	NH		8.34, d (8.6)
<i>L</i> -proline	CO	170.4	
	α	59.9	4.67, d (7.8)
	β	32.0	1.94, m; 1.61, m
	γ	20.9	1.65, m; 1.41, m
	σ	45.6	3.28, m

944

945

946 **Table 4** ^1H (500 MHz) and ^{13}C NMR (125 MHz) data of compounds **5–9** (J in Hz)

No.	5 ^a	6 ^b	7 ^b	8 ^b	9 ^b
2	7.99, brs	7.79, brs	7.72, brs	7.71, brs	7.69, d (5.7)
3					6.30, d (5.7)
5	4.83, d (2.2)	4.59, d (7.7)	4.51, d (1.7)	4.27, d (7.6)	4.57, d (7.7)
6	1.37, m	1.64, m	1.32, m	1.97, m	1.63, m
7	1.77, m	2.03, m; 1.45, m	1.81, ddd (12.9, 12.2, 6.7); 1.72, m	2.15, m; 1.75, m	2.03, m; 1.46, m
8	2.66, m	2.66, m; 2.55, m	2.63, dd (18.6, 6.7); 2.56, dd (11.4, 7.0)	2.48, m	2.64, m; 2.54, dt (18.2, 4.8)
9	4.31, d (13.7); 4.27, d (13.7)	4.33, d (13.5); 4.29, d (13.5)	4.34, d (13.0); 4.30, d (13.0)	4.35, d (13.6); 4.27, d (13.6)	
10	1.63, m; 1.41, m	1.85, m; 1.28, m	1.64, m; 1.44, m	1.21, m; 1.13, m	1.84, m; 1.28, m
11	1.04, t (7.3)	0.98, t (7.3)	1.00, t (7.4)	0.97, t (7.4)	0.98, t (7.5)
12	3.40, s	3.44, s	3.44, s	3.44, s	
13			3.54, s	3.54, s	

^aCD₃OD; ^bCDCl₃

947

948 **Table 5** ^{13}C NMR (125 MHz) data of compounds **5–13**

No.	5 ^a	6 ^b	7 ^b	8 ^b	9 ^b	10 ^b	11 ^b	12 ^b	13 ^b
2	155.2	152.8	152	152	155	151.3	153.5	152.6	152.7
3	126.0	125.2	125.3	125.4	116.5	125.5	121.4	125.2	125.1
4	179.2	179.5	177.6	177.6	180.3	174.5	177.2	178.2	178.6
4a	125.2	123.5	123.6	121.0	125.0	120.1	123.8	123.5	122.1
5	62.3	69.0	70.8	73.4	69.0	111.4	124.0	64.3	68.8
6	42.0	41.5	41.2	36.4	41.4	140.4	141.5	42.3	72.4
7	22.7	23.3	21.8	19.8	23.3	26.9	134.0	21.6	27.9
8	28.8	27.0	27.9	23.3	27.0	26.2	118.1	27.2	24.8
8a	168.8	165.6	166.6	166.0	165.7	162.4	155.1	165.6	165.6
9	67.0	66.1	66.5	66.5		66.6	66.6	66.2	66.2
10	25.3	25.3	24.6	22.0	24.5	29.8	28.5	138.2	29.3
11	11.9	11.3	12.1	12.2	11.3	12.1	15.7	116.1	6.8
12	58.9	59.2	59.1	59.2		59.1	59.0	59.2	59.2
13			60.2	58.1					

^aCD₃OD; ^bCDCl₃

949

950

951 **Table 6** ^1H (500 MHz) data of compounds **10–13** (CDCl_3 , J in Hz)

No.	10	11	12	13
2	7.71, s	7.95, s	7.78, s	7.78, s
5	6.37, s	8.03, d (2.2)	4.93, brs	4.62, s
6	/	/	2.39, m	/
7	2.39, t (9.2); 2.75, t (9.2)	7.51, dd (8.6, 2.2)	2.05, m; 1.85, m	1.96, m; 1.80, m
8	2.75, t (9.2)	7.38, d (8.6)	2.67, dd (6.0, 3.4); 2.62, dd (10.3, 6.2)	2.81, m; 2.51, m
9	4.34, brs	4.43, d (1.0)	4.33, brd (13.5); 4.29, brd (13.5)	4.33, brd (13.6); 4.29, brd (13.6)
10	2.17, dd (7.3, 7.1)	2.75, q (7.6)	6.08, m	1.89, m; 1.58, m
11	1.09, t (7.4)	1.28, t (7.6)	5.22, dd (1.3, 1.3); 5.19, dd (5.3, 1.3)	1.04, t (7.5)
12	3.46, s	3.48, s	3.46, s	3.45, s

952

953 **Table 7** ^1H (500 MHz) and ^{13}C NMR (125 MHz) data of compound **14** (CDCl_3 , J in Hz)

No.	δ_{C}	δ_{H}
1	162.1	
3	76.3	4.55, m
4	31.5	2.90, dd (16.1, 2.9); 3.06, dd (16.1, 11.6)
4a	141.7	
5	119.5	6.82, d (8.0)
6	134.7	7.46, dd (8.0, 8.0)
7	111.1	6.92, d (8.0)
8	161.4	
8a	114.8	
9	73.6	3.62, dd (10.3, 5.4); 3.70, dd (10.3, 4.9)
10	59.7	3.44, s
11	56.3	3.94, s

954

955

956 **Table 8** IC₅₀ values of compounds **10**, **11**, **32**, **36**, and **41** against the induced proliferation of induced-T and
 957 B lymphocytes, and their CC₅₀ values for lymphocytes

Sample	T cells	B cells	lymphocytes
	IC ₅₀ (μM)		CC ₅₀ (μM)
10	>20	8.0	>20
11	>20	20.0	>20
32	3.1	6.0	>20
36	>20	16.7	>20
41	12.1	16.7	>20
Dex	1.9	1.0	0.2

958 **Table 9.** Inhibition rates of compounds **1–3** and **15–17** against the cell proliferation of ConA-induced T
 959 lymphocytes and LPS-induced B lymphocytes, and cell validity treated with these compounds

Group	c (μM)	Inhibition rate (%)		Cell validity (%)	Group	c (μM)	Inhibition rate (%)		Cell validity (%)
		T	B				T	B	
1	40	16.5±1.5	20.4±6.3	90.7±4.0	15	40	28.8±5.8	29.0±12.2	80.2±1.8
	20	11.4±6.4	18.9±7.5	86.3±2.1		20	26.4±6.3	23.0±4.3	89.9±7.5
2	40	32.8±6.8	30.6±6.2	89.8±7.9	16	40	20.7±4.3	20.5±10.6	96.2±1.1
	20	23.8±0.9	24.9±8.6	100.0±2.4		20	13.1±2.7	19.3±4.6	101.8±6.9
3	40	26.5±3.3	22.6±9.6	89.9±4.4	17	40	16.3±4.3	20.7±6.9	100.0±8.5
	20	15.7±7.9	11.0±4.9	87.7±7.4		20	10.1±4.4	11.5±3.1	94.0±5.6
Dex	2	45.2±4.9	68.6±1.5	36.9±2.2	Con				100±9.5

960 **Table 10.** IC₅₀ values of active compounds against the proliferation of HaCaT cells

Sample	IC ₅₀ (μM)	Sample	IC ₅₀ (μM)
9	35.0±3.1	33	33.9±2.8
10	30.9±2.7	34	32.2±3.4
13	31.1±2.6	35	31.5±2.4
19	29.70±3.3	37	32.0±2.2
22	32.3±1.5	38	25.2±1.6
24	32.5±2.0	39	32.6±3.6
25	35.1±1.9	40	32.9±3.4
28	29.1±1.7	41	27.7±2.5
30	31.2±4.1	MTX	26.4±1.4
32	27.0±1.3		